

<https://helda.helsinki.fi>

On the sources of uncertainty in the sub-3 nm particle concentration measurement

Kangasluoma, J.

2017-10

Kangasluoma, J & Kontkanen, J 2017, ' On the sources of uncertainty in the sub-3 nm particle concentration measurement ', Journal of Aerosol Science , vol. 112 , pp. 34-51 . <https://doi.org/10.1016/j.jaerosci.2017.07.002>

<http://hdl.handle.net/10138/307934>

<https://doi.org/10.1016/j.jaerosci.2017.07.002>

cc_by_nc_nd

acceptedVersion

Downloaded from Helda, University of Helsinki institutional repository.

This is an electronic reprint of the original article.

This reprint may differ from the original in pagination and typographic detail.

Please cite the original version.

On the sources of uncertainty in the sub-3 nm particle concentration measurement

J. Kangasluoma and J. Kontkanen

Department of Physics, P.O. Box 64, 00014, University of Helsinki, Helsinki, Finland

Abstract

The number of experiments characterizing sub-3 nm aerosol particle dynamics has increased significantly over the recent years. In these experiments, it is essential to know/determine size resolved particle number concentrations accurately. Despite particle concentration measurement being relatively simple experiment, it can contain large uncertainties from various sources in the sub-3 nm size range. In this study we aim to identify and examine some of these sources. We simulated four different condensation particle counters (CPCs) (TSI 3777, ADI vWCPC, Airmodus A11 and an ideal CPC with d50 (lowest detection threshold) of 1.5 nm) and one differential mobility analyzer (DMA) (TSI nano DMA) and study the resulting uncertainties when using them to measure three different particle size distributions. First, we show that Poisson uncertainty \sqrt{N}/N represents the statistical uncertainty in all CPC and DMPS counting experiments. Second, the state-of-the-art DMA-CPC particle sizing system is examined with respect to counting statistics. Third, the performance of the instruments is assumed to be well-known, and instrumental non-idealities and the inversion routine are assessed. Fourth, ± 0.5 nm offset is inserted to the CPC d50, and its effect on the measured particle concentration is examined. Our results highlight the importance of knowing the CPC d50 accurately to narrow down the particle concentration uncertainty. Furthermore, the results show that the current DMA-CPC measurements are subject to considerable counting uncertainty in low particle concentration environments. Based on the analysis we summarize suggestions for further research and instrumental development for more accurate sub-3 nm particle concentration measurements in the future.

1 Introduction

In recent years, great efforts have been made to understand the formation and growth of sub-3 nm particles in the atmosphere (Jiang et al., 2011c; Kulmala et al., 2013; Bianchi et al., 2016; Sipilä et al., 2016) and in controlled conditions in chamber studies (Kirkby et al., 2011; Almeida et al., 2013; Ehn et al., 2014; Kirkby et al., 2016). Simultaneously, a need has emerged for the optimization of specific industrial applications and particle synthesis methods related to phase transition of vapor to liquid or solid nanoparticles (Alanen et al., 2015; Kangasluoma et al., 2015; Carbone et al., 2016; Nosko et al., 2016; Wang et al., 2016, 2017). The current view is that atmospheric gas-to-particle conversion occurs via formation of molecular clusters from low-volatile vapors and their subsequent growth to larger aerosol particles (e.g. Kulmala et al., 2014). The growth of the clusters is hindered e.g. by coagulation losses to the aerosol population and diffusional losses to the near-by surfaces, both of which are the highest for the smallest sizes. Therefore, particle populations with a continuous formation of the molecular clusters are typically characterized by a strong decrease in the particle concentration with the increasing particle size in the sub-3 nm size range (Jiang et al., 2011c; Kulmala et al., 2013).

A direct measurement of the particle formation includes both chemical characterization of the nucleating species by mass spectrometric methods (Smith et al., 2010; Jokinen et al., 2012; Ehn et al., 2014; Lopez-Hilfiker et al., 2015) and a size resolved particle concentration measurement by condensation particle counting methods (Jiang et al., 2011c; Kulmala et al., 2013). The time dependent and size resolved particle concentrations are further used to infer the size resolved particle nucleation and growth rates (Jiang et al., 2011c; Kuang et al., 2012; Kulmala et al., 2013; Lehtipalo et al., 2016; Tröstl et al., 2016). Despite the recent advances, large uncertainties exist in the particle concentration measurements in the sub-3 nm size range. The particle concentration measurement uncertainties

49 arise, for example, from low particle counting statistics (Jiang et al., 2011b), from chemical
50 composition dependent variation in the lowest threshold diameter of the particle counters (Jiang et
51 al., 2011b; Kangasluoma et al., 2014) or from unknown charging probabilities in the sub-3 nm size
52 range (Premnath et al., 2011). The uncertainties in the measured particle concentrations accumulate
53 into the derived parameters, such as the nucleation and growth rates.

54 Almost all of the recent experimental efforts to characterize sub-3 nm particle dynamics rely
55 on diethylene glycol (DEG) based condensation particle counters (CPCs) (Iida et al., 2009; Jiang et al.,
56 2011c; Kirkby et al., 2011; Kuang et al., 2012; Yu et al., 2012; Almeida et al., 2013; Kulmala et al., 2013;
57 Yu et al., 2014; Alanen et al., 2015; Kangasluoma et al., 2015; Bianchi et al., 2016; Kirkby et al., 2016;
58 Kontkanen et al., 2016; Nosko et al., 2016; Wang et al., 2016; Kontkanen et al., 2017; Wang et al.,
59 2017). However, a well-known challenge of a DEG based CPC is that the particle detection efficiency
60 at mobility diameters below 3 nm largely depends on the chemical composition of the particles.
61 Previously e.g. Jiang et al. (2011b), Kangasluoma et al. (2014) and Kangasluoma et al. (2016b) have
62 determined the detection efficiency of the DEG based CPCs in the laboratory for clusters of variable
63 chemical composition. The results show that the difference between the lowest and the highest d50
64 (diameter at which the detection efficiency is 50% of the plateau value) of the DEG based CPC can be
65 approximated to be at maximum 1 nm. This translates to an offset value of ± 0.5 nm in the d50 value,
66 if the particle chemical composition is completely unknown. However, this source of uncertainty can
67 be minimized almost to a negligible value, when the CPC is calibrated with the same type of particles
68 as sampled in the experiment (Kangasluoma et al., 2015). Unfortunately, this is currently not possible
69 for many applications, such as for atmospheric observations.

70 In addition to the uncertainties related to the particle composition dependent detection
71 probability, there are numerous other factors causing difficulties in the accurate measurement of the
72 sub-3 nm particle concentrations. The CPC calibrations rely on charged test particles as they can be
73 linked to the concentrations determined with electrometers, while there are no established
74 concentration reference instruments for electrically neutral sub-3 nm particles. Furthermore, there is
75 a lack of sources capable of producing electrically neutral and size selected particles with known
76 chemical composition. As heterogeneous nucleation of charged particles takes place at lower
77 supersaturation than that of neutral particles (Winkler et al., 2008; Kangasluoma et al., 2016b;
78 Kangasluoma et al., 2017), uncertainty in the d50 arises if charging state of the calibration aerosol is
79 not similar to the charging state of the measured aerosol. This source of uncertainty is most
80 pronounced when the measured aerosol is mostly electrically neutral and CPC calibration is conducted
81 with charged test particles. Also, if large but unknown fraction of the measured particles is charged,
82 the effect of charge on the d50 is difficult to take into account even with a proper calibration. Only
83 few sub-3 nm CPC calibrations with the size selected, electrically neutral particles have been
84 conducted so far (Kangasluoma et al., 2016b; Kangasluoma et al., 2017). They suggest an increase of
85 0.1 – 0.5 nm in the d50 for the neutral particles compared to the identical experiment with the charged
86 particles. Thus, if the effect of charge on the d50 is not known in a given experiment, one could assume
87 an increase of 0.3 nm to the d50, obtained from calibration with charged particles, which can be taken
88 into account in the data inversion. Thereby the d50 offset can be estimated as ± 0.2 nm, which covers
89 the range of d50 variation of current experimental data.

90 Brownian motion causes uncertainty in the sub-3 nm particle concentration measurements in
91 two ways. On one hand, the small particles are lost to sampling line walls very efficiently, which causes
92 uncertainty in the measured particle concentration. However, the size dependent losses can be
93 characterized experimentally and the effect can be corrected as long as there is at least some part of
94 the particles that penetrate through the sampling lines. The most straightforward way to overcome
95 this challenge is to use core sampling in the sampling line, which can increase the transmission of sub-
96 3 nm particles almost to unity (Kangasluoma et al., 2016a). On the other hand, the particle diffusion
97 hinders the particle size classification resolution (e.g. Stolzenburg and McMurry, 2008) of differential

mobility analyzers (DMAs). The challenges arise, when a DMA with a wide transfer function (Ω_{DMA}) relative to the sampled particle size distribution is used, as discussed later in this study.

Diffusion charging of aerosol particles larger than 10 nm in size is rather well understood (e.g. Wiedensohler and Fissan, 1990), and similarly is chemical ionization via charge transfer at the molecular scale (e.g. Eisele and Tanner, 1993; Lindinger et al., 1998). However, the transition from the chemical charge transfer to the diffusion based charging taking place at the size scale of molecular clusters is not well understood. Therefore, possibly a large source of uncertainty is related to the charging efficiency of sub-3 nm particles and molecular clusters, which depend on the chemical composition of the clusters themselves and the ions responsible for their charging. Overall, this process is essential in the electrical mobility analysis based measurements. Few studies in the past have probed the charging characteristics of the sub-3 nm particles. Alonso et al. (1997) presented experimental data on bipolar charging probabilities of sub-3 nm particles, which underestimates the charging probability by up to a factor of 2 from the Fuchs diffusion based charging theory. Premnath et al. (2011) studied the charge transfer from the small clusters back to the vapor molecules, which is not taken into account in the regularly used diffusion charging theories, and found out that the charge transfer is dependent on both cluster size and chemistry. Due to a lack of experimental data the charge transfer processes at cluster level are not well understood, and these effects are often not discussed as a source of uncertainty in the sub-10 nm particle concentrations measurements. Alas, for the same reason, our study does not discuss charging related uncertainties any further. This topic requires a separate comprehensive analysis combining theoretical and experimental methods.

Lastly, uncertainties in the concentration obtained from CPC experiments can originate from the number of counted particles. To probe this source of uncertainty, we assume that particle sampling and counting is a Poisson process. A process needs to fulfil three requirements to be a Poisson process (Bertsekas and Tsitsiklis, 2002):

1. Time homogeneity: at each time interval τ the probability to detect N counts needs to be the same i.e. detection of a count is equally likely at all times.
2. The number of detected counts, N , during a time interval τ is independent of the history of detected counts outside this interval τ , i.e. a detected count does not affect the detection of another count.
3. During a short time interval: the probability to detect a count is roughly $\lambda\tau$ (λ is the counting rate), the probability to not detect any counts is roughly $1 - \lambda\tau$, and when τ becomes smaller, the probability to detect two or more counts becomes negligible.

In a Poisson process counting experiment, which is performed multiple times, the resulting number of counts is a normal distribution around the mean value of count number. For a Poisson process the distribution standard deviation, σ , equals to \sqrt{N} . The relative uncertainties ([%]) are obtained when σ or \sqrt{N} are normalized with N . Generally, σ/N is defined as the statistical uncertainty, while \sqrt{N}/N is the counting (Poisson) uncertainty. In Poisson process these are equal.

For CPC counting the conditions 1 and 2 are satisfied, if the particles in the sample air flow can be considered to be distributed randomly (due to Brownian motion) and uniformly. The condition 3 is satisfied, as there are no processes creating simultaneous counts i.e. each particle is sampled and detected separately.

The purpose of this study is to numerically investigate the uncertainties related to the particle counting with three different size distributions and four CPCs in five different case studies. The main focus is placed upon the challenges arising from narrow input particle number size distributions, when they are sampled with a theoretical CPC parametrized based on Kangasluoma et al. (2017) and Vanhanen et al. (2011). The CPC counting statistics related uncertainty is first studied in a general CPC counting experiment, and then examined based on a published state-of-the-art instrument utilizing the DMA-CPC technique. The effect of non-ideality and offset in the d_{50} diameter on the detected particle concentration are both studied in cases when a DMA is applied upstream of the CPC, and

without the DMA. Finally, the uncertainties in the particle sizing method utilizing supersaturation scanning with a specific CPC are examined. The study presents the first comprehensive uncertainty analysis on the sub-3 nm particle concentration measurements. Furthermore, suggestions are provided for the future instrumental development to improve the accuracy of sub-3 nm particle concentration measurements. It must be stressed that this study does not criticize any previous work, nor claim anything on the reliability of any specific previous or forthcoming data. Rather, the previous scientific works are appreciated as the inspiration for this analysis.

2 Methods

2.1 Instrumentation used in the numerical simulations

The online sub-3 nm particle sizing methods can be divided into two types of methods, named here as a differential mobility analyzer – condensation particle counter (DMA-CPC) method and a particle size magnifying (PSM) method. The DMA-CPC method functions as follows: the sampled particles are first guided to an aerosol charger. The aerosol, which is assumed to be brought to charge equilibrium in a charger (e.g. Wiedensohler and Fissan, 1990), is further guided to a DMA (Hewitt, 1957; Knutson and Whitby, 1975; Chen et al., 1998), leading to a charged and monodisperse particle population downstream of the DMA. A CPC is used to count the number concentration of the particles. This is a traditional differential mobility particle sizer (DMPS, e.g. Wiedensohler et al., 2012) method used to monitor size resolved particle concentrations.

Sub-3 nm particle measurements can be performed using the DMA-CPC method with a TSI nano DMA (Chen et al., 1998). We base our analysis on the system described in Jiang et al. (2011b), in which the TSI nano DMA is operated at flow rates $Q_a = 2$ liters per minute (lpm) and $Q_s = 20$ lpm for aerosol and sheath flows, respectively. The resolution (R) of the DMA (see Flagan, 1999) is defined as the ratio between the selected mobility and the transfer function peak width (full width at half maximum, FWHM) as follows: $R = Z/\Delta Z_{FWHM}$. In our case with the TSI nano DMA, the corresponding resolution is 3 – 4 (Jiang et al., 2011a). The CPC used in Jiang et al. (2011b) was a modification from a TSI ultrafine 3025A CPC (Stolzenburg and McMurry, 1991), in which the working fluid was changed from butanol to DEG, and the original counting optics were removed and replaced by another follow-up CPC (Jiang et al., 2011b; Kuang et al., 2012; Wimmer et al., 2013) as DEG is typically not able grow the particles to large enough size to be detected with the optics. In the TSI ultrafine 3025A/3776 CPC design the aerosol flow rate in the condenser is 0.3 lpm, out of which 0.03 lpm (in 3025A) or 0.05 lpm (in 3776) contains the particles and is directed to the counting optics through a narrow capillary and the rest is filtered and saturated sheath flow around the particle flow. This flow arrangement has two implications on the analysis of this study: with the sheathed condenser design the d50 curve will be steep as the particles are exposed to a rather constant supersaturation, while the dilution lowers the counting statistics by a factor of 10 with the 3025A compared to TSI 3022, and by a factor of 33 compared to TSI 3772, where all of the sampled particles are directed to the optics with the flow rates of 0.3 lpm and 1 lpm, respectively.

The PSM method refers to a mixing type CPC technology initiated by Okuyama et al. (1984), and further developed by Seto et al. (1997) and Gamero-Castano and Fernández de la Mora (2000) and their successors. In this method, the CPC is often named as a particle size magnifier as this instrument was initially used to study the particle growth. The current commercial PSMs use DEG as a working fluid which only initiates the particle growth (Vanhanen et al., 2011), thereby requiring another CPC for the particle counting. The particle sizing in the PSM is based on the fact that heterogeneous nucleation probability at a fixed supersaturation depends on the particle size (Fletcher, 1958). Thus, by scanning the supersaturation in the PSM, the particle size distributions can be inferred from the total concentrations measured with the different d50 diameters (Lehtipalo et al., 2014). A

combination of Airmodus A10 PSM and A20 butanol CPC is commercially available as the A11 system and the analysis of this study is performed for this setup.

A possible instrument in the future sub-3 nm particle studies is the recently published water based CPC (Hering et al., 2016), which can achieve particle detection near 1 nm. Compared to a conventional water CPC (Hering et al., 2005), the new versatile water CPC (vWCPC) has three temperature stages instead of the previous two. With this kind of setup, it can reach supersaturations high enough to detect particles as small as 1 nm. The vWCPC is a non-sheathed CPC, which subsequently makes the d50 curve more flat relative to for example the original TSI 3025A design.

In this study we investigate the performance of three CPCs introduced above (TSI 3777, Airmodus A11, and vWCPC), to detect particle concentration, and the DMA-CPC and the PSM method to measure particle size distribution. In addition to the real CPCs, an ideal CPC with d50 at 1.5 nm is included as a reference in the analysis to distinguish between the uncertainties related to the CPC d50 curve and other factors.

Figure 1 upper panel presents the d50 curves of the three CPCs, which are published in Kangasluoma et al. (2017) for the vWCPC and 3777 and in Vanhanen et al. (2011) for the A11. The fits to the curves are according to the following equation:

$$\eta_{cpc}(d_p) = A * e^{(-e^{(-k*(dp-dp_0))})} \quad (1)$$

where A is the d50 curve plateau value height, d_{p0} is the diameter offset and k is a curvature parameter.

2.2 Test particle size distributions

Three test particle size distributions (SDs) were selected for the study: one from ambient experiments (SD1, Jiang et al., 2011c), one from a flow tube reactor experiment (SD2, Yu et al., 2012) and one from an engine combustion exhaust emission study (SD3, Alanen et al., 2015) (Figure 1 lower panel). The three SDs were chosen to represent the full variability in the number size distributions in the sub-3 nm size range to examine the effect of the sample SD on the uncertainty in the measured particle concentrations. Therefore, these selected SDs contain only particles smaller than 10 nm, which is not realistic e.g. for atmospheric conditions. However, larger Aitken or accumulation mode particles would only increase the offset concentration detected by all the CPCs, which is not relevant for this study as our focus is only on sub-3 nm sizes.

The following characteristics should be noted on the test size distributions: we have normalized all the distributions to peak concentrations of unity for simplicity. Furthermore, in SD1 the concentration decreases from the peak value of 1 at 1 nm to 0.01 at 2 nm, exhibiting a steep negative concentration gradient as a function of particle size. Notably this gradient coincides with the size range of the CPC d50 diameters. This kind of SD is typical for the systems where the clusters are constantly formed from precursor vapors (Jiang et al., 2011c; Kulmala et al., 2013). Also, it should be noted that in SD1 the concentration decreases towards zero below 1 nm, which is not realistic in ambient particle SD. This does not, however, affect the results of the calculations as the CPCs of this study do not detect any particles below 1 nm. In a similar manner, SD2 exhibits a steep concentration gradient, but in this case the gradient is positive at the CPC d50 size range. The SDs similar to this can be observed in particle reactors, where uniform and rapid particle formation and growth takes place, and the particles have a uniform time to form and grow (Yu et al., 2012; Ezell et al., 2014). SD3 presents a much smaller concentration gradient than the first two SDs with a peak concentration at 4 nm. These three size distributions are used in three of the four case studies. In the second case study these SDs are not used, but instead the SD required to achieve certain statistical uncertainty in the CPC counting is calculated.

2.3 Data inversion

In the calculations presented in this study we focus on two parameters: the concentration detected by the CPCs and the inverted concentration from the detected concentration, which gives the particle SD when using the DMA-CPC or PSM method.

CPC

The concentration detected by the CPC (C_{tot}) directly monitoring a particular test SD was calculated as:

$$C_{tot} = \int_0^{\infty} \frac{dC}{dd_x} * \eta_{CPC}(d_x) * dd_x \quad (2)$$

where dC/ddx ([arbitrary unit scaled to unity at peak concentration]) denotes the particle number size distribution and $\eta_{CPC}([\%])$ is the d50 curve for a given CPC shown in Figure 1. The uncertainties in C_{tot} for different CPCs were investigated in case study 1 and 3 (see the next section).

DMA-CPC

In the DMA-CPC method the DMA transfer function was calculated according to Stolzenburg and McMurry (2008). A concentration detected by the DMA-CPC system ($C_{det}(d_p)$, [arbitrary unit]) monitoring a test SD was calculated as:

$$C_{det}(d_p) = \int_0^{\infty} \frac{dC}{dd_x} * \eta_{CPC}(d_x) * \Omega_{DMA}(d_p, d_x) * dd_x \quad (3)$$

where $\Omega_{DMA}([\%])$ is the DMA transfer function. From the $C_{det}(d_p)$ the inverted SD, $C_{inv}(d_p)$ ([arbitrary unit, same scale as of C]), is calculated as:

$$C_{inv}(d_p) = \frac{C_{det}(d_p)}{\eta_{CPC}(d_p) * A * \int_0^{\infty} \Omega_{DMA}(d_p, d_x) dd_x} \quad (4)$$

where η_{CPC} is the detection efficiency of the CPC at a given diameter, $\int_0^{\infty} \Omega_{DMA}$ is the integral over the DMA transfer function and A is the d50 curve plateau value. We assume all particles to be singly charged, as in the sub-3 nm size range the probability of double or more charging is close to zero (Wiedensohler and Fissan, 1990). Note that in the inversion, the use of η_{CPC} and Ω_{DMA} as single values contain the assumption that the SD does not significantly change over the size range where the d50 curve increases from 0 to A, or in the size range of the Ω_{DMA} . On the contrary, the $C_{det}(d_p)$ takes into account the shape of the SD, d50 and Ω_{DMA} . This is the case in all real DMPS experiments too. In cases studies 3 and 4 we examine the validity of this assumption by sampling the strongly varying SDs as a function of the particle size.

When a CPC of a DMPS system records particle counts, the following parameters need to be taken into account in the inversion: particle sampling losses, charging probability, DMA penetration and CPC detection efficiency, the product of which is the particle size dependent total penetration ($P_{tot}(d_p)$) of the system. In this study, we follow the DMPS system presented in Jiang et al. (2011b). The total penetration of this system is depicted in Figure 2. As shown in the introduction part, the counting

statistics can be assumed to follow Poisson statistics, i.e. the number of counts in a given time interval is known on average, but the time interval between two counts is random. Thus, during a fixed time period the obtained number of counts can deviate from the average. When many identical counting experiments are conducted, the obtained counts follow a normal distribution. The standard deviation of this distribution describes the statistical uncertainty of the counting experiment. It can be shown that the counting uncertainty, which follows Poisson statistics is \sqrt{N}/N where N is the number of counts (see Figure 3). For example, 10 and 100 counts counted by the CPC yields $\pm 31\%$ and $\pm 10\%$ counting uncertainty, respectively. The individual counts from particles detected by the CPC of a DMPS system can be calculated from

$$N = C_{SD}(d_p) * P_{tot}(d_p) * t * Q_o \quad (5)$$

where $C_{SD}(d_p)$ is the sampled concentration of particles, $P_{tot}(d_p)$ is the total penetration of the DMPS system, t is the counting time i.e. the time the DMA spends at one voltage, and Q_o is the flow rate through the optical detector of the CPC. This system is examined in the case study 2.

PSM

The inversion for the PSM method follows the methodology presented in Lehtipalo et al. (2014). However, the difference in our inversion is that we use experimentally defined Ω_{PSMS} as compared to the selected Ω_{PSM} shapes of Lehtipalo et al. (2014). Figure 4 (left hand side panel) shows the PSM calibration, which is obtained by feeding size selected tungsten oxide particles to the PSM, and scanning the supersaturation by scanning the saturator flow rate (Q_{sat}). The calibration curves are normalized to unity at $Q_{sat} = 1$ lpm. From the normalized curves the Ω_{PSMS} are obtained by subtracting the calibration curves from each other so that the obtained size bins are 1.1–1.2 nm, 1.2–1.3 nm and so on. To these Ω_{PSMS} , Gaussian curves are fitted (Figure 4 right hand side panel). Q_{sat} is converted to diameter (x-axis in Figure 4 right hand side panel) by finding out Q_{sat} for which the detection efficiency is 50% of the maximum value for each diameter. The diameter for each size bin was selected as the diameter corresponding the maximum value of each Ω_{PSM} . These Ω_{PSMS} can be readily used in the calculations similarly as the DMA Ω s. The concentration detected by the PSM method is given by

$$C_{det}(d_p) = \int_0^\infty \frac{dC}{dd_x} * \Omega_{PSM}(d_p, d_x) * dd_x \quad (6)$$

From $C_{det}(d_p)$, the inverted concentration is calculated as

$$C_{inv}(d_p) = \frac{C_{det}(d_p)}{\int_0^\infty \Omega_{PSM}(d_p, d_x) dd_x} \quad (7)$$

In case study 5 we examine the PSM inversion, and the effect of diameter offset in Ω_{PSM} to the inverted SDs.

2.4 Case studies

Five case studies were performed to address various aspects affecting the uncertainties in measured sub-3 nm particle concentrations. In cases 1 and 2 we examine statistical uncertainties of CPC and DMPS counting, and briefly discuss the statistical uncertainties related to cases 3-5. In cases 3-5 the uncertainty in the measured particle concentrations was studied 1) by assuming well-known d50 curves or 2) by inserting ± 0.5 nm offset to the d50 curve. In the calculations in which no d50 offset

was assumed, the d50s are the ones presented in Figure 1. In the calculations in which the offset is inserted to the d50 curve, it is conducted so that the initial d50 curve is shifted by + 0.5 nm, which is taken as the reference d50 curve, and then ± 0.5 nm offset is inserted to this reference curve. The reasoning for this is that the d50s presented here (and in the manufacturer brochures) are the best case curves i.e. the lowest d50 values obtained using particles that are easily detected with the instrument. The offset value of ± 0.5 nm is taken from our previous studies (Kangasluoma et al., 2014; Kangasluoma et al., 2016b) to reflect the case where composition of the sampled particles is unknown. In real experiments the d50 offset can be larger, for example ± 0.75 nm, if the effect of charge and relative humidity are not considered, but also smaller (even negligible) if the particle composition and charging state are known and taken into account in the instrument calibration. For this study, the absolute value of the d50 offset is important in the sense that if it was larger, the resulting uncertainties in the detected particle concentrations would be larger, and vice versa. It must be highlighted that the uncertainty can be narrowed down by a proper instrument calibration as shown for example in Kangasluoma et al. (2015), and data presented here do not represent any specific experiment.

Case 1: Statistical uncertainty in CPC sampling

We performed Monte Carlo simulations to test the validity of our subsequent non-statistical analysis. In the simplest case, the real CPCs sample a particle distribution representing the SD1. The number of sampled particles from the SD, N , was set to 10, 100, 1000, 10000 and 100000 on average. As sampling of particles in our study is assumed to be a Poisson process, in each simulation N is a random number from normal distribution around N with $\sigma = \sqrt{N}$. The probability of detection for each sampled particle was according to the CPC d50 curve, with uniform detection probability. This simulation was conducted 10000 times for each N , and the number of counted particles was analysed. From the distribution of counted particles the uncertainty can be calculated in two ways: statistical uncertainty as σ/N , or Poisson counting uncertainty as \sqrt{N}/N .

Case 2: DMA-CPC statistical uncertainty

In this case study the performance of the complete DMPS system, described in Section 2.1, with respect to counting of sub-3 nm particles and counting statistics is examined. The only studied uncertainty is the counting uncertainty, and other variables are assumed to be well-known. In this case study, we determine which sampled size distribution yields counting uncertainty smaller than 5%, 15% and 50%, which correspond to 400, 44 and 4 counts, respectively (Figure 3). The SD is directly obtained from Eq. 5 by solving it for $C_{SD}(d_p)$. In the calculations t is set to 15 s and Q_o to 0.03 lpm. The value of t is calculated from Jiang et al. (2011b) assuming constant t at each DMA voltage. In many DMPS systems t might not be constant as a function of size but the counting time is increased for the smallest particles. However, the results from this study scale linearly with t , i.e. doubling t reduces the required concentration to half.

Case 3: CPC sampling

In the third case study the four CPCs (3777, A11, vWCPC, and ideal CPC) directly sample the three SDs (Eq. 2), first assuming no error in the d50 curve, and then including a ± 0.5 nm offset to the d50 curve as explained in Section 2.4. When no offset is assumed, the parameters of interest are the ratio between the detected concentration and the real concentration above the nominal d50, and the fraction of the detected particles that are smaller than the nominal d50 of a CPC. When the ± 0.5 nm offset is inserted to the d50, the detected concentration is compared to a number which the CPC should detect in an ideal case, that is, the concentration above the nominal d50 in the SD.

Case 4: DMA-CPC sampling

In the fourth case study a DMA is placed upstream of the CPC and the DMA-CPC system samples the test SDs with the four different CPCs (Eqs. 3 and 4). We do not consider any uncertainties related to particle sampling or charging. Similar analysis is performed as in the second case study: firstly the inverted concentrations are analyzed with respect to the initial SD assuming no error in the d50, and secondly ± 0.5 nm offset is added to the d50. The inverted concentrations are compared to the initial SDs, the parameter of interest being the ratio of these two.

Case 5: PSM sampling

In the last case study, the uncertainties related to the PSM method are examined similarly as in the cases 3 and 4 by using Eqs. (6) and (7). Firstly the deviations in the inverted concentrations from the initial SDs are studied, when no error in the d50 is assumed, and secondly the Ω_{PSMS} of the A11 are exposed to an offset of ± 0.5 nm. It is assumed that all the Ω_{PSMS} shift with a constant value of ± 0.5 nm, which, however, might not be a completely accurate assumption.

3 Results and discussion

3.1 Case 1: Statistical uncertainty in CPC sampling

An example figure of the first simulation is shown in Figure 5, the top panel showing one size distribution with $N = 1000$ (on average) where on top the SD1 and CPC d50 curves are plotted. The second panel presents the counted particle frequency for the 10000 simulations for the vWCPC with $N = 1000$. By calculating the two uncertainties, statistical and counting, from the distributions such as the one shown in the second panel, we obtain numbers in the Table 1. The uncertainty of the counted particles follows Poisson counting uncertainty as shown in the Table 1 (similar values for σ/N and \sqrt{N}/N), so, the uncertainty is only dependent on the number of counted particles. This is expected from the properties of the Poisson process: if we consider only particle of one size, its detection can be assumed to follow Poisson statistics. If we consider particles of two different sizes with unequal detection rates which are independent of each other, their sum still follows Poisson statistics. This can be generalized to n different independent sizes of particles with unequal detection rates, the sum of which follows Poisson statistics. Based on this, we can make a simple calculation for a usual CPC counting experiment: let us assume CPC optics flow rate of 1 lpm, counting time of 1 s and sampled concentration of 100 particles cm^{-3} . This gives us counted particles of $N = 1660$ (on average) and counting uncertainty of $\pm 2.5\%$. Based on the relatively good counting statistics in a normal CPC counting experiments, we can conclude that the counting, and thus, statistical uncertainties are quite low in most CPC counting experiments. Possibly excluded situations are CPCs with very low optics flow rates or/and environments with very low particle concentrations, such as arctic areas or clean room facilities. In these cases the counting statistics are easily improved by longer counting time.

Importantly, the previous still holds when the particles are sampled with a DMPS system: the sum of particles with different detection rates (inside the width of a DMA transfer function originating from different charging and DMA transmission probabilities, and changing size distribution) obey the Poisson process and statistics. The fact that particle counting with both a CPC and a DMPS follow Poisson statistics generalizes the statistical uncertainties of concentration measurements to Poisson uncertainty. In general, this is useful observation, since very seldom the measured processes are slow enough to obtain sufficient amount of scans with a DMPS system to calculate the σ/N , and the number of counted particles in the DMPS system is not often high enough to neglect the counting uncertainties for a single measurement.

Tables 2 and 3 list the statistical uncertainties obtained for the parameters listed in Tables 4 and 5 for SD1 at various N values. Table 4 lists the ratio of detected concentration and true concentration above the CPC d50, while Table 5 lists the ratio of detected concentration and detected concentration below the CPC d50. We selected these two parameters to describe the CPC

performance in measuring particle concentrations at sizes close to the CPC d50. Statistical uncertainties of these parameters do not follow Poisson uncertainty, as they are calculated from two variables that are dependent on each other. Based on the current study we cannot generalize these uncertainties quantitatively, but only qualitatively as follows: the uncertainties are lower when the number of counted particles is higher. On the other hand, the uncertainties are lower when the CPC d50 is the steeper or the particle SD is flatter. The former is trivial and observed in Tables 2 and 3. The latter can be reasoned as follows: a counting experiment with an ideal CPC does not suffer from the non-idealities of the parameters of Tables 4 and 5, and the steeper the d50 curve, the smaller the possibility of counting particles below the nominal d50. Similarly, the steeper the SD, the more important parameter the CPC d50 is in determining the particle concentration accurately, as is obvious from later parts of this study.

We do not study the magnitudes or uncertainties of these uncertainties that do not follow Poisson uncertainties more deeply because they are very case dependent and depend strongly on the SD shape, d50 shape, counted particle number and factors causing d50 offset. Due to the previous, more general approach nor more deep analysis has not been done also for the numbers obtained in Figures 8 and 10, and in Tables 6a and 6b. However, we can conclude that, at least for such parameters listed in Tables 4 and 5, if number of detected particles is $1e4$ or more, the statistical uncertainties of the parameters are less than 5%. This is most probably a good estimate for the data of Figures 8 and 10, and Tables 6a and 6b, since those parameters are calculated from two similar (but not independent) variables as in Tables 2 and 3.

All in all, in most normal CPC and DMPS experiments, and our cases 3 and 5, the statistical uncertainties can be assumed to be equal to Poisson uncertainty, and all derivative parameters of this study to have statistical uncertainties smaller than 5% if number of counted particles is more than $1e4$.

3.2 Case 2: DMA-CPC counting uncertainty

In the third case study, we assume that all the instrumental parameters are well-known, and we only examine the uncertainty related to counting statistics in the DMA-CPC system. The DMPS system follows the performance of the only published DMPS system measuring particles down to 1 nm by Jiang et al. (2011b) (Figure 2). Figure 6 shows the particle SDs with the concentrations required to achieve 4, 44 and 400 counts to the CPC of the examined system. These counts represent the number of counts in any counting experiment which yield counting uncertainties smaller than 50%, 15% and 5%. It can be seen from the figure that the studied DMPS system requires the sampled particle concentration of approximately $1e7\text{ cm}^{-3}$ at 1 nm to achieve the counting uncertainty smaller than 5%. At 3 nm, the respective concentration is approximately $1e5\text{ cm}^{-3}$. To achieve the counting uncertainties of smaller than 15% and 50%, the respective concentrations are approximately one and two orders of magnitudes lower than the ones for 5%. This result clearly implies that to obtain statistically reliable data (or any data at all), one needs very high particle concentrations at the DMPS system inlet. There exist at least two methods to rather easily increase the counting statistics of the studied DMPS system: using a detector with a higher optics flow rate and optimizing sampling line penetration. For example, the TSI 3777 (Kangasluoma et al., 2017) offers the detected flow rate of 0.15 lpm and the A11 system the flow rate of 1 lpm, which enable better counting statistics by a factor of 5 and 33, respectively, compared to the TSI 3025A. The sampling system presented in Kangasluoma et al. (2016a) practically removes inlet line losses, producing almost a tenfold increase to the signal at 1 nm. By implementing the improved counting statistics by a factor of 33 by replacing the 3025A with an A11 and improved sampling line, the required concentrations presented in Figure 6 would be approximately two orders of magnitude smaller. Further improvements would be obtained by improving the transmission of the DMA, or by improving the charging efficiency, which at the current stage will require more fundamental research.

3.3 Case 3: CPC sampling

For the three studied SDs, the ratios of the detected concentration to the real concentration above the d50 of each CPCs are listed in Table 4. The errors in the detected concentrations, indicated as the ratio between the CPC response to the ideal performance (ratio's deviation from unity), result from the changing size distribution at the size range where the d50 increases from 0 to A. Therefore, the errors are the largest (-12% to 272%) for the vWCPC as its d50 curve increases from 0 to A in the largest diameter range (see Fig. 1). The d50 curves of the 3777 and A11 are similarly steep but placed at different concentration gradient of the SDs. Because the concentration gradient is larger at the d50 of the 3777 compared to the A11, the errors are also larger for the 3777 (-4% – 32%) than for the A11 (-1% or less).

The fractions of the detected particles that are smaller than the nominal d50 of CPC, are given in Table 5 for different SDs. As expected, the ideal CPC does not detect anything below its d50 but the real CPCs detect particles that are smaller than the nominal d50 of a CPC due to the non-ideal d50 curves. The smallest fractions (less than 2%) are observed for the SD3 in which the concentration gradient is positive and relatively small at the size of the CPC d50s, and most of the particles in the SD are larger than the d50 values. For the SD2 with a larger but positive concentration gradient at the d50 sizes, the fractions are also relatively low, less than 10%. However, when the gradient is large and negative, as is the case for SD1, a significant fraction of the detected particles is below the nominal d50 values. For vWCPC the fraction of the particles detected below the d50 value is the highest (67%) as the d50 curve reaches to much smaller diameters as its nominal d50 value. The d50 curves of 3777 and A11 exhibit similar steepness, but as the d50 of the 3777 is at the region of higher concentration gradient for the SD1, the fraction of the particles detected below d50 is larger (37%) than the value of A11 (12%) (Table 5). These results imply that non-idealities of the d50 curve can cause significant measurement error, particularly in the cases when the SD is narrow. In the worst case it can cause either an overestimation up to some hundred percent (SD1) or an underestimation of some ten percent (SD2) (Tables 4 and 5).

Next, ± 0.5 nm error was applied to the d50 curve, and the detected concentrations are compared to the real concentration above the nominal, correct d50 values. Tables 6a and 6b present the concentration ratios for the d50 offsets of +0.5 nm and -0.5 nm, respectively. Errors in the detected concentrations are again the smallest for the SD3, approximately $\pm 15\%$, due to the smallest concentration gradient and the fact that most particles in the SD are larger than the d50s. For SD2, in which the peak concentration is close to the d50 values, the ± 0.5 nm error in d50 curve causes errors of approximately -70% to +130% to the detected concentrations. The errors in the detected concentration are the largest for the SD1, ranging from -98% to > 1000%. This is because in SD1 there is a strong negative concentration gradient in the size range of the d50s of all the CPCs. The observed errors in the detected concentrations imply strongly that the knowledge on the d50 is crucial when determining the particle concentrations in systems where particle formation takes place, producing steep particle size distributions. The magnitude of the error is determined by the combination of how CPC d50 is located relative to the SD and the shape of the d50 curve. The stronger the concentration gradient is, more uncertainty in the detected concentration is induced, if d50 is not exactly known. Most importantly, universal uncertainty in the detected concentration cannot be given even if the uncertainty in the d50 can be known, as the concentration uncertainty always depends on the sampled particle SD.

3.4 Case 4: DMA-CPC sampling

In case study 4 a Ω_{DMA} is included in between the particle SD and CPC, and inverted concentrations are studied. The inverted concentrations are limited to values where the detection efficiency of the CPC is larger than 5% and where the size distribution is more than 0.1% from the peak value. This is to avoid the most extreme and uncertain values, which probably would not be used in a real experiment either. Figures 7a-c present the inverted SDs and the ratios of inverted SDs to the initial SD for different SDs with all CPCs. In these plots the d50 is assumed to be known, and all errors in the inverted concentrations arise from the fact that the particle concentration changes in the size range of the Ω_{DMA} and d50 curve.

From Figure 7 it can be observed that the ideal CPC underestimates the concentration close to the d50 value for all the SDs. This is because the DMA transmits also particles smaller than the d50, which are not detected by the CPC. At the sizes where all the particles are larger than the ideal CPC d50, the ideal CPC, like all other CPCs, overestimates the detected concentration by approximately 0 – 15%. This results from the fact that the particle concentration in the SD decreases exponentially as a function of size, and therefore the concentration at the Ω_{DMA} maximum value does not represent the average concentration over the whole Ω_{DMA} width. For the real CPCs, two processes are competing below the CPC d50 value: the concentration is underestimated because particles smaller than the d50 are transmitted through the DMA, since the concentration gradient is strongly negative in the SD at the d50 size. Simultaneously the concentration is overestimated because the particles larger than the d50 size are also transmitted, and they are detected at a higher probability than the value of $\eta_{CPC,dp}$ (CPC detection efficiency at a given diameter) used in the inversion. Correction to the detected particle concentration due to $\eta_{CPC,dp}$ increases with the decreasing particle size, and the net effect leads to the overestimated particle concentration. This overestimation is most pronounced for the SDs 2 and 3 in which the concentration gradient at the sizes of d50 is positive, and therefore relatively more particles larger than the d50 are transmitted through the DMA.

Thus, in the case of the DMA-CPC system the instrumental non-idealities alone can cause significant error in the detected concentration. In our calculations, these errors range from -60% up to 560% depending on the diameter, the initial SD and the characteristics of the CPC. The largest overestimations are associated to diameters where the CPC detection efficiency is lower than $0.5 \cdot A$ (half of the d50 curve plateau value). The overestimation is smaller for the vWCPC than for the 3777 and A11 because its d50 is the least steep. As mentioned above, for these calculations we used only diameters at which the CPC detection efficiency was larger than 5%. However, to avoid the observed underestimation and overestimation problems in data inversion, using diameters at which the CPC detection efficiency is larger than $0.9 \cdot A$ is suggested. At diameters where $\eta_{CPC} > 0.9 \cdot A$, the error was smaller than 15% for SD1 and smaller than 2% for SD2 and SD3. The high uncertainties arise again from the steep SDs as a function of particle size. The magnitude of the errors cannot be estimated, if the size distribution is not known before the inversion routine, which is always the case in real experiments.

Next, ± 0.5 nm error is introduced to the d50 values of the CPCs. The ratios of inverted concentration to the initial size distribution in this case are shown in Figures 8a-c. The observed deviations in the inverted concentration from the real concentration follow rather similar patterns for all the CPCs and SDs. The uncertainties range from -100% to > 1000% and they are again most pronounced for the SD1 due to the strong negative concentration gradient at the d50 sizes. These results further show that if the d50 of a CPC is not exactly known for the studied system, the safest way is to use a DMA-CPC system that starts from a diameter where the CPC detection efficiency is above 90% of the plateau value for the worst case d50. With the DEG based CPCs this limit lies somewhere around 2 – 3 nm (Kangasluoma et al., 2014).

3.5 Case 5: PSM sampling

In the last case study, we investigate the performance of the A11 method in retrieving the SDs by means of scanning the supersaturation. Following the similar analysis as in the case studies 3 and 24 we first analyze the inversion without uncertainties in the Ω_{PSMS} , and subsequently add a ± 0.5 nm error to the Ω_{PSMS} presented in Figure 4. The analysis is again limited to the SD diameters, where the concentration is larger than 0.1% of the peak concentration. As in the case of the DMA-CPC inversion, the PSM inversion includes uncertainties resulting from the fact that the particle concentration changes significantly within the width of a Ω_{PSM} . As seen from Figure 9, SD1 is overestimated at 2 nm while SD2 is underestimated at this size. This is due to Ω_{PSMS} which are skewed toward larger sizes. On the other hand, the inversion of the rather flat SD3 includes relatively small errors. The errors in the inverted concentrations ranged from -15% to +70%.

The error of ± 0.5 nm in the Ω_{PSMS} causes error in the measured concentrations at all sizes in the inverted concentrations for the PSM method, while for the DMA-CPC the errors are only at the size range close to the CPC d50 (see Section 3.2). Thus, in the case of the PSM method, the initial SD mostly defines the magnitude of uncertainty in the inverted concentration (Figures 9 a-c). The largest errors in the inverted concentrations are observed for the SD1, ranging from -100% up to 5000%. The concentration can also be under- and overestimated for a single SD as shown for SD2 when there is ± 0.5 nm offset in the Ω_{PSMS} . These, rather large, uncertainties are obtained because the inverted concentration with shifted Ω_{PSM} is directly compared to the initial size distribution. It corresponds to the case in which the instrument user needs a size classified concentration at a given (mobility) diameter. Estimating the associated uncertainties for a given experiment is challenging because the uncertainty depends on the initial SD. In this case study, all the uncertainties are assumed to be in the particle concentration, which leads to very high uncertainties. Therefore, a more convenient approach in the PSM method would be to include only counting and other experimental uncertainties in the concentration uncertainty, and include the Ω_{PSM} related (particle composition, charge and sample flow relative humidity) uncertainty in the size bin uncertainty. In the following nucleation and growth rate calculations the size bin uncertainty would be directly the corresponding size uncertainty of the size at which the nucleation or growth rate was calculated. In our case study, this would mean that instead of having uncertainty from -100% to 5000% in the concentration with exact diameter, the concentration uncertainty would be from -15% to 70% and the diameter uncertainty ± 0.5 nm. In this case the SDs inverted from PSM method would be supersaturation equivalent diameters, which would make data intercomparison more straightforward. On the other hand, this could complicate further analysis, such as interpreting particle formation and growth rates calculated from the concentrations or the comparison between the concentrations measured with the PSM and other instruments.

4 Conclusions

In this study, the uncertainties in the sub-3 nm particle concentration measurement were examined. Several parameters that affect the accuracy of the measurement were identified, including the initial size distribution (SD), the steepness of the detection efficiency (d50) curve of the detector, the d50 accuracy with respect to the particle composition and charge (how well the CPC calibration test aerosol represents the measured aerosol), and detector counting statistics. Based on the analysis, the following conclusions can be drawn:

- 1) In all CPC and DMPS experiments the Poisson statistics uncertainty (\sqrt{N}/N) describes the statistical uncertainty of the counted particles.
- 2) Achieving the counting uncertainty smaller than 5% with the studied DMPS system requires high particle concentrations ($> 1\text{e}5 \text{ cm}^{-3}$), which are not present in many systems.

- 3) CPCs can sample particles smaller than their nominal d50 diameter due to non-ideal d50 curve, which, depending on the sample SD can lead to overestimation or underestimation of the particle concentration. In our cases concentration error was in the range of -12% to 272%.
- 4) In the data inversion, using a single value for the DMA and PSM transfer functions (Ω_{DMA} and Ω_{PSM}) and CPC detection efficiency (η) is inevitable but it causes errors in the inverted concentrations. This results from the fact that the particle concentration can change significantly within the width of a Ω_{DMA} and Ω_{PSM} .
- 5) The steeper function of particle size the initial SD is, the larger the uncertainties in the concentration measurement are.
- 6) The largest uncertainties in the inverted concentrations with the DMA-CPC can be avoided by limiting the size range of the instrument only to diameters where the CPC detection efficiency is more than 90% of the plateau value. By using smaller CPC detection efficiency values than 90% the concentration error can be up to 500% due to instrumental non-idealities.
- 7) If the properties of the sampled particles are unknown, the largest uncertainties in the measured concentrations are associated in the PSM sizing method (in our cases from -100% to 5000% in the whole sizing range with ± 0.5 nm d50 uncertainty), since the transfer functions, Ω_{PSM} s, are directly exposed to the uncertainty in the η . With the DMA-CPC method unknown particle properties cause uncertainty to the measured concentration only in the size range close to the d50 (in our cases from -100% to 1000% with ± 0.5 nm d50 uncertainty).
- 8) Uncertainties are always case dependent

Future research to reduce the simulated uncertainties presented above, should focus on:

- 1) Designing CPCs with steeper d50 curves.
- 2) Finding nontoxic CPC working fluid capable of sub-3 nm particle detection and with a minimal composition and charge dependency, and homogeneous droplet production.
- 3) Building DMAs with a higher sizing resolution ($R > 5$) with reasonable transmission which are applicable to field experiments.
- 4) Improving DMPS counting statistics by
 - a. Using CPCs with larger optics flow rates.
 - b. Minimizing the sampling losses.
- 5) Studying sub-3 nm charging efficiency

Further, the implications of the particle concentration measurement uncertainties on the derivative parameters, such as the particle nucleation and growth rate (Kulmala et al., 2012), should be studied.

Acknowledgements

The authors thank Prof. Tuukka Petäjä, Prof. Markku Kulmala and M.Sc Joonas Vanhanen for fruitful discussions. This work was partly funded by Maj and Tor Nessling foundation (grant 201700296) and Academy of Finland (Center of Excellence Program projects 1118615 and 139656).

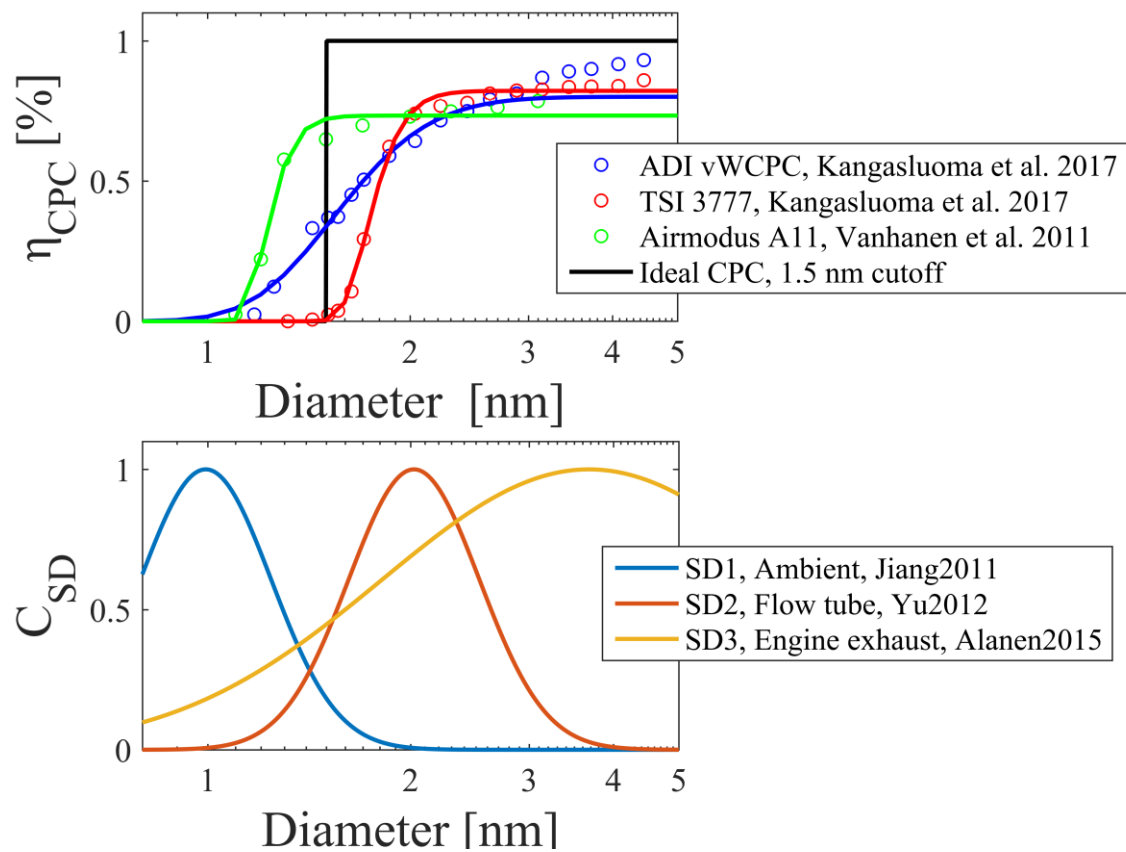


Figure 1. The CPC d50 curves and test particle size distributions. Concentration unit for the size distributions is arbitrary.

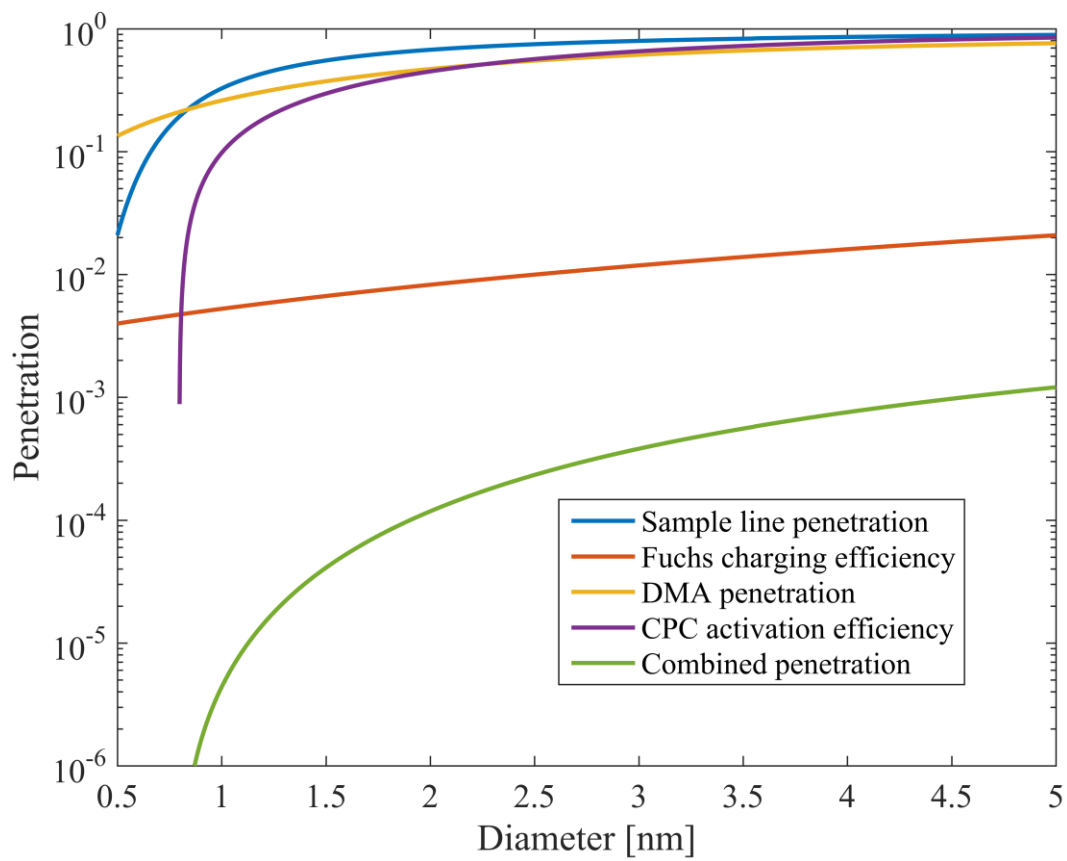
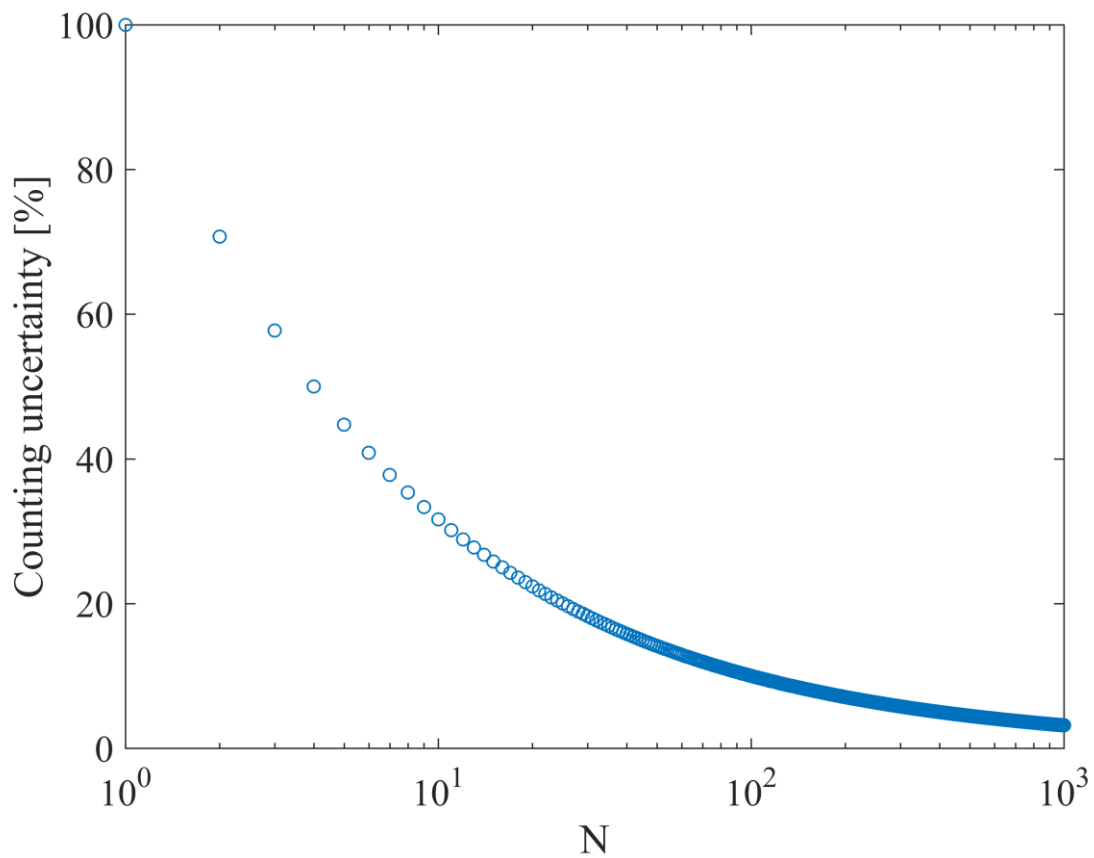
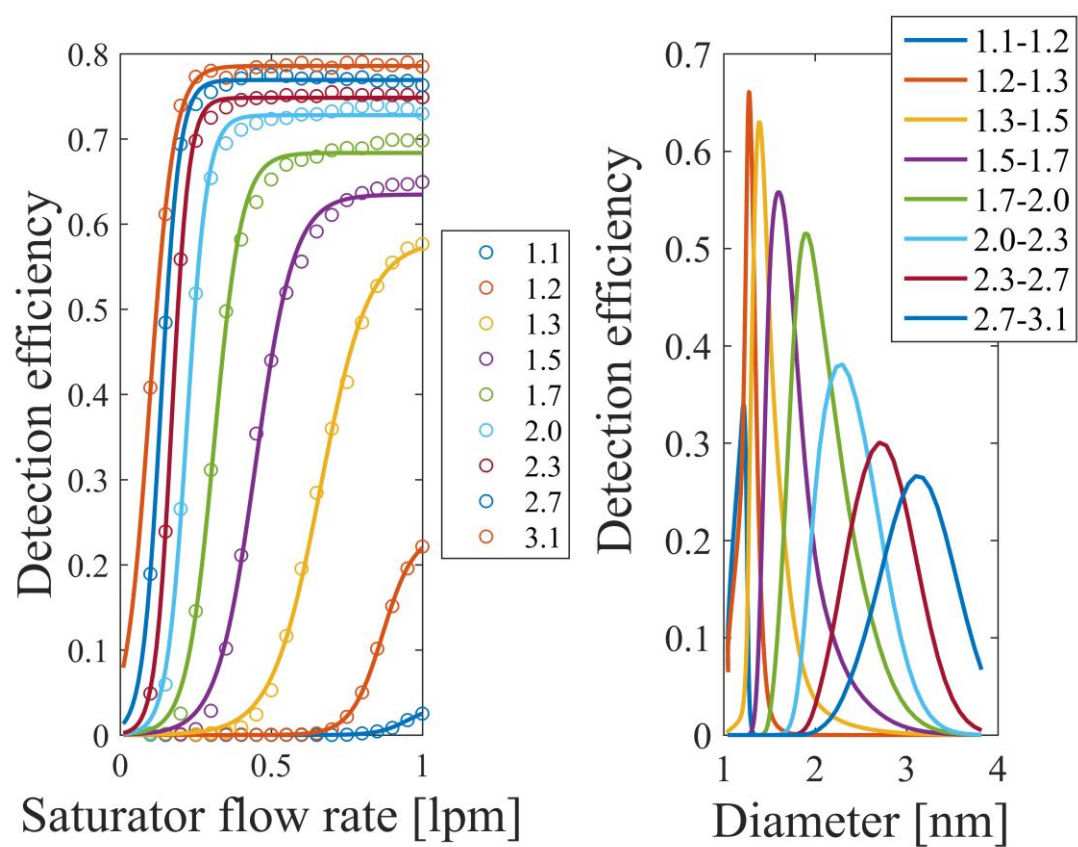


Figure 2. Penetrations of the DMPS system in case study 3.



669 Figure 3. Counting statistics uncertainty for Poisson distribution. N is the number of counts.



670
671 Figure 4. PSM method calibration and transfer functions. Different colors represent different sizes (in
672 nm).
673

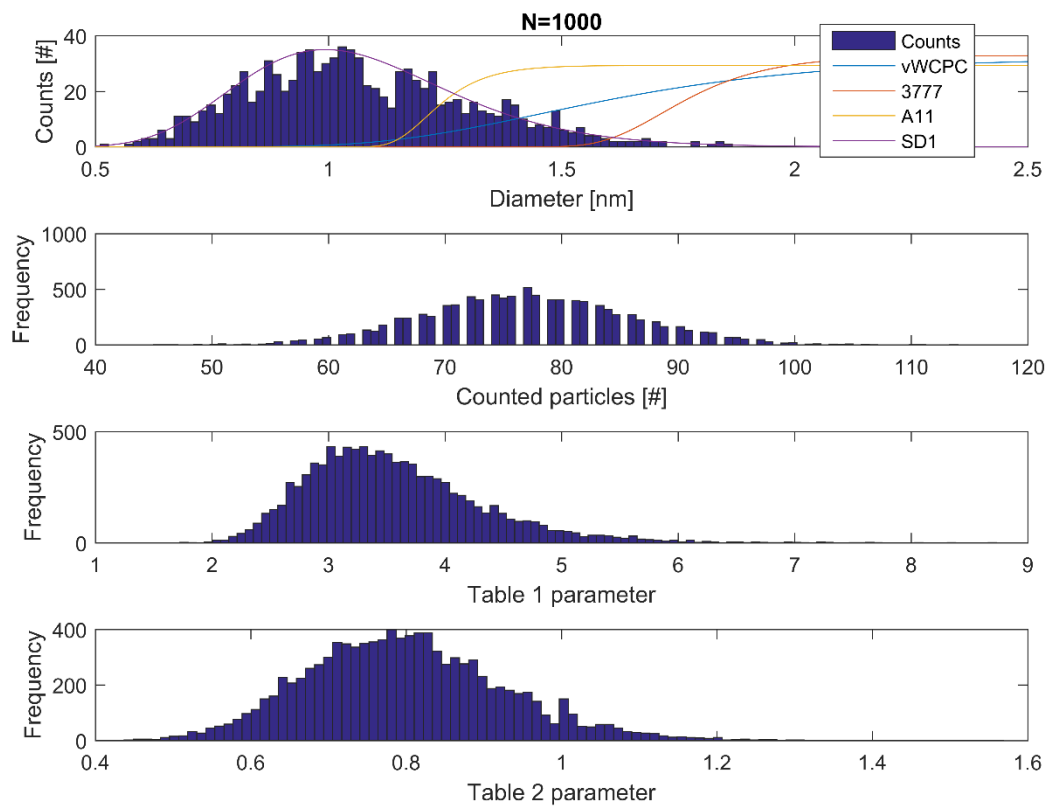


Figure 5. Upper panel: Example simulated distribution of SD1 with 1000 counts and on top plotted CPC d50 curves. Second panel: counted particles by vWCPC in the 10000 simulations. Third panel: Table 1 parameter for the vWCPC and SD1. Fourth panel: Table 2 parameter for the vWCPC and SD1.

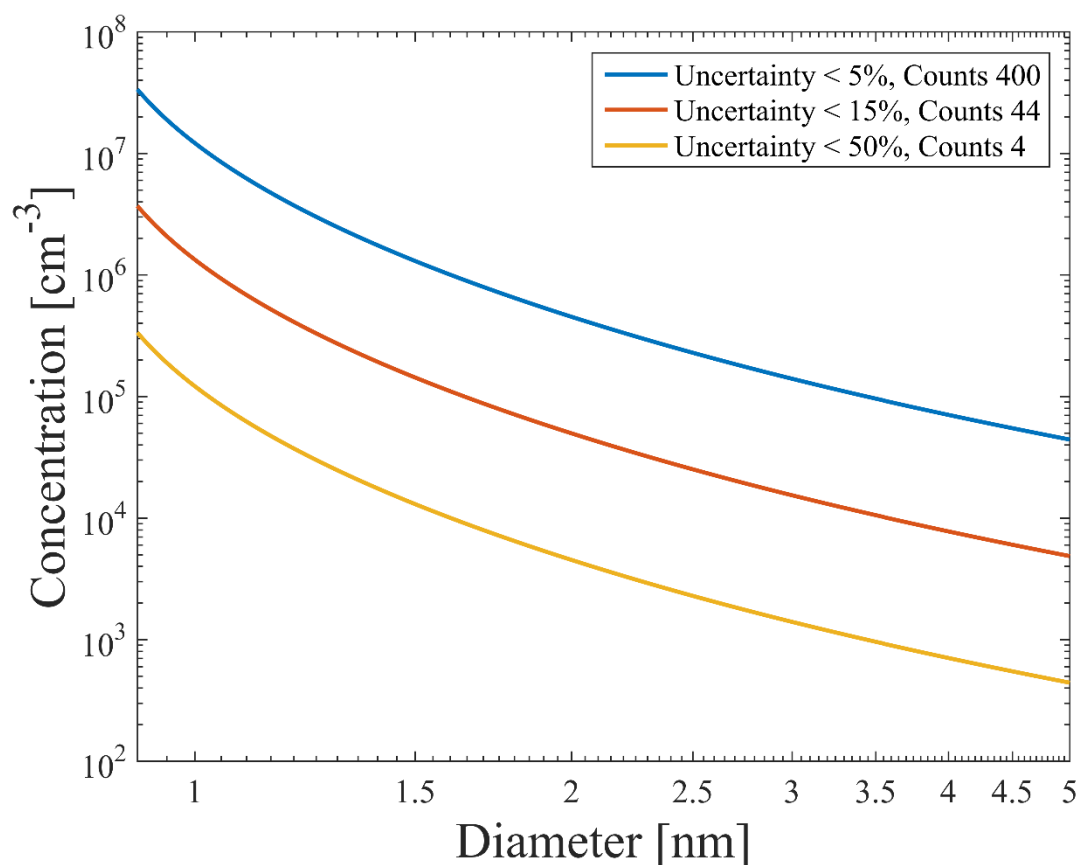
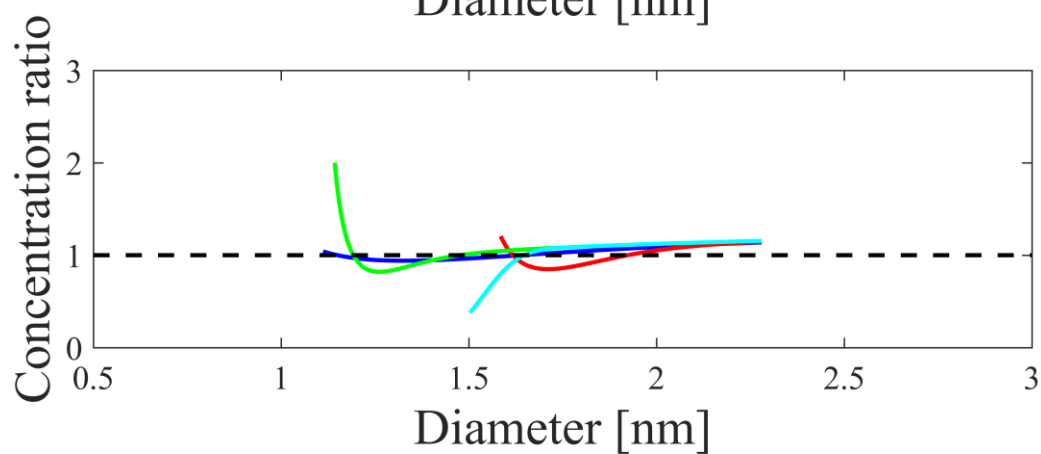
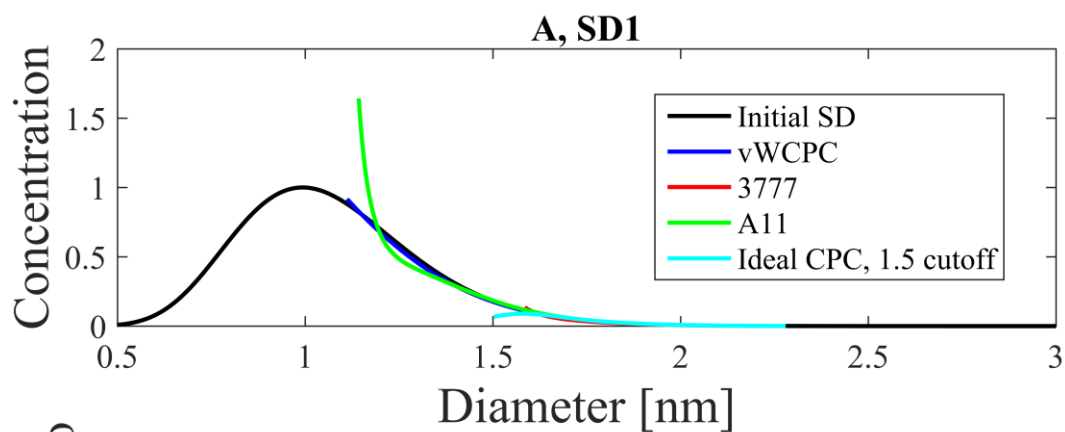
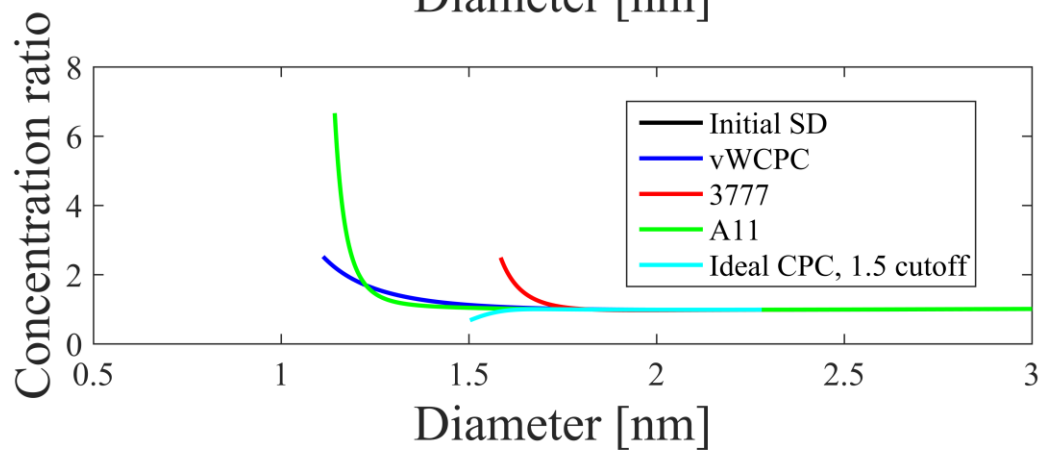
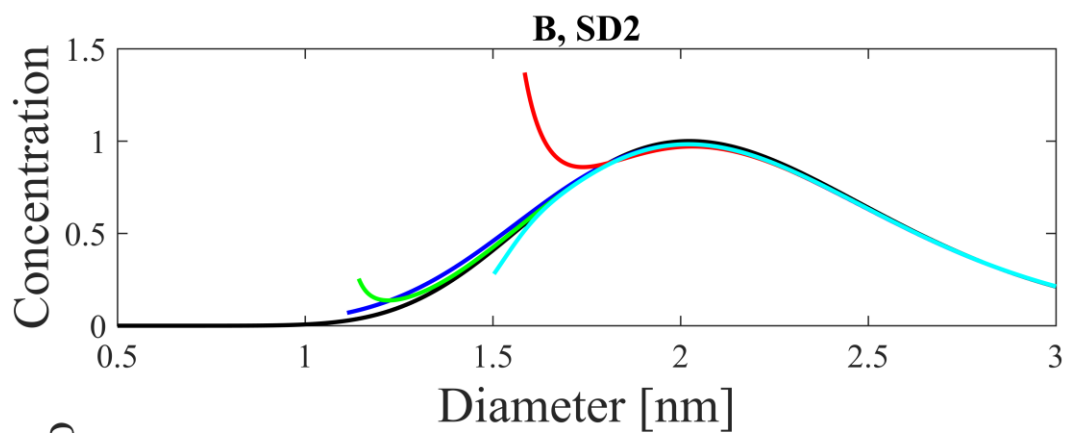


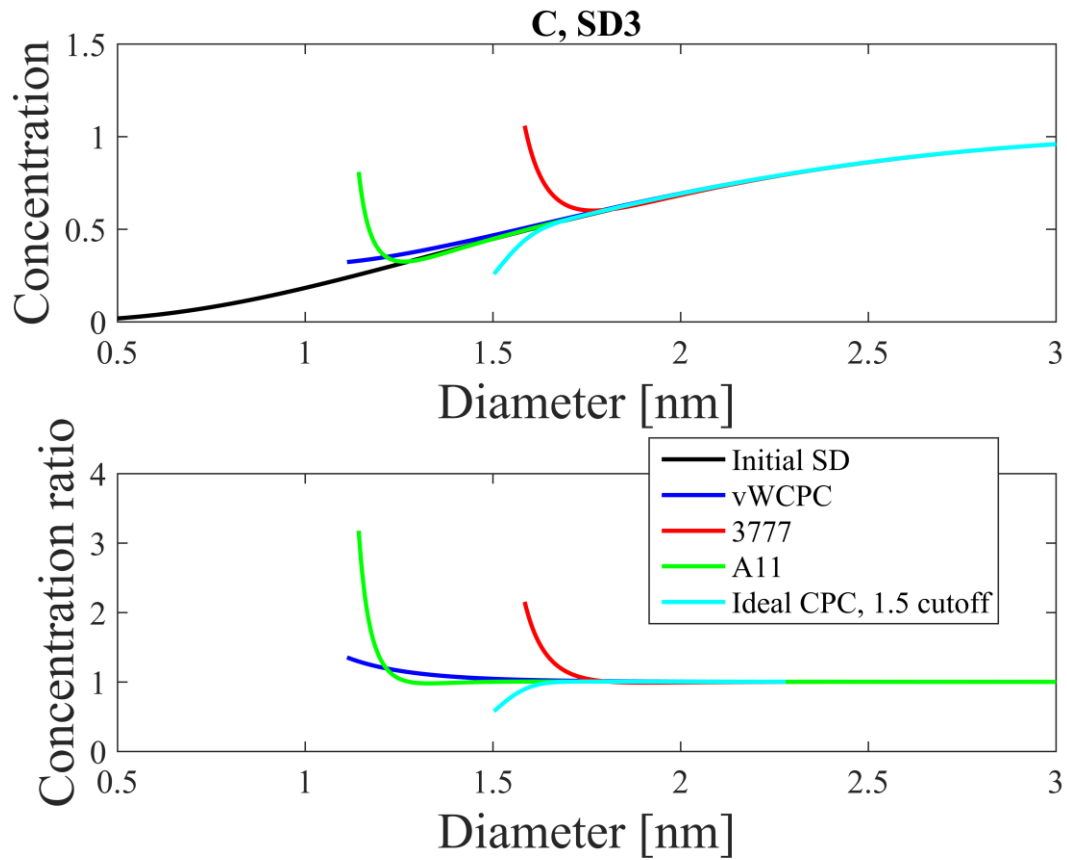
Figure 6. The DMA-CPC sampling an arbitrary particle size distribution. Lines show the particle concentration required to reach statistical uncertainty smaller than 5%, 15% and 50% with the DMPS published by Jiang et al. (2011b).



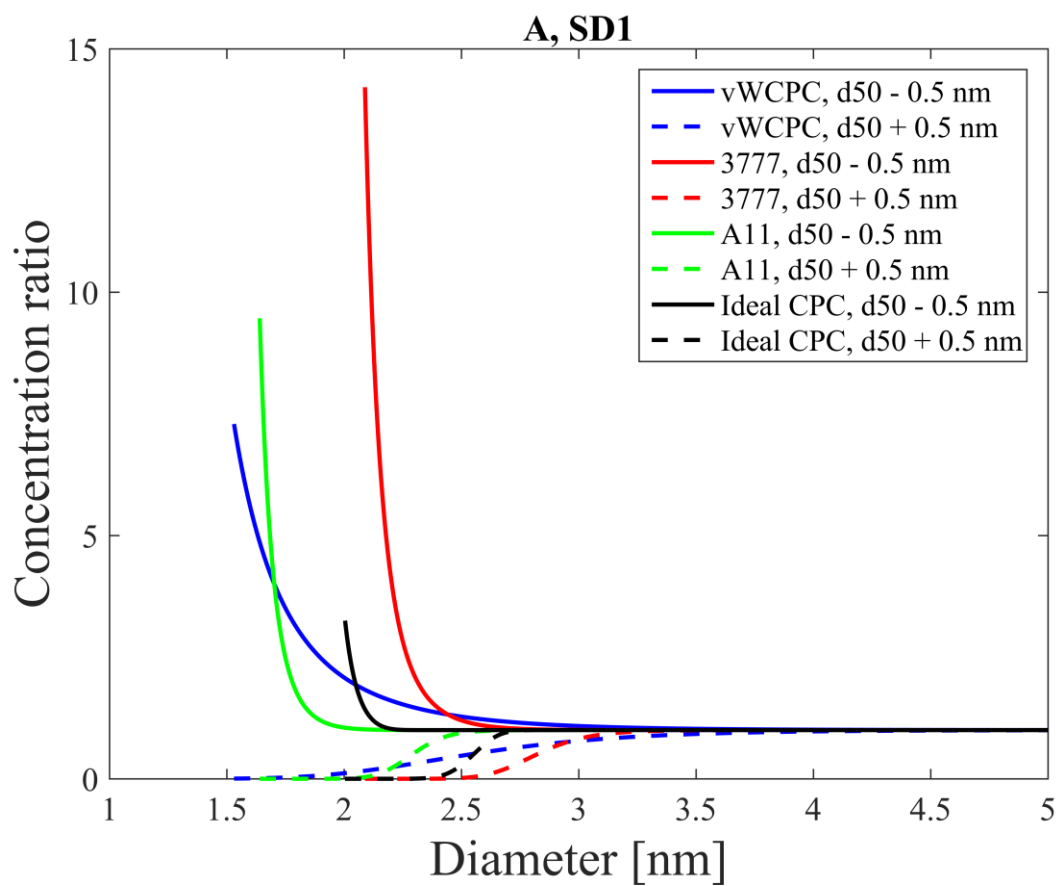
684



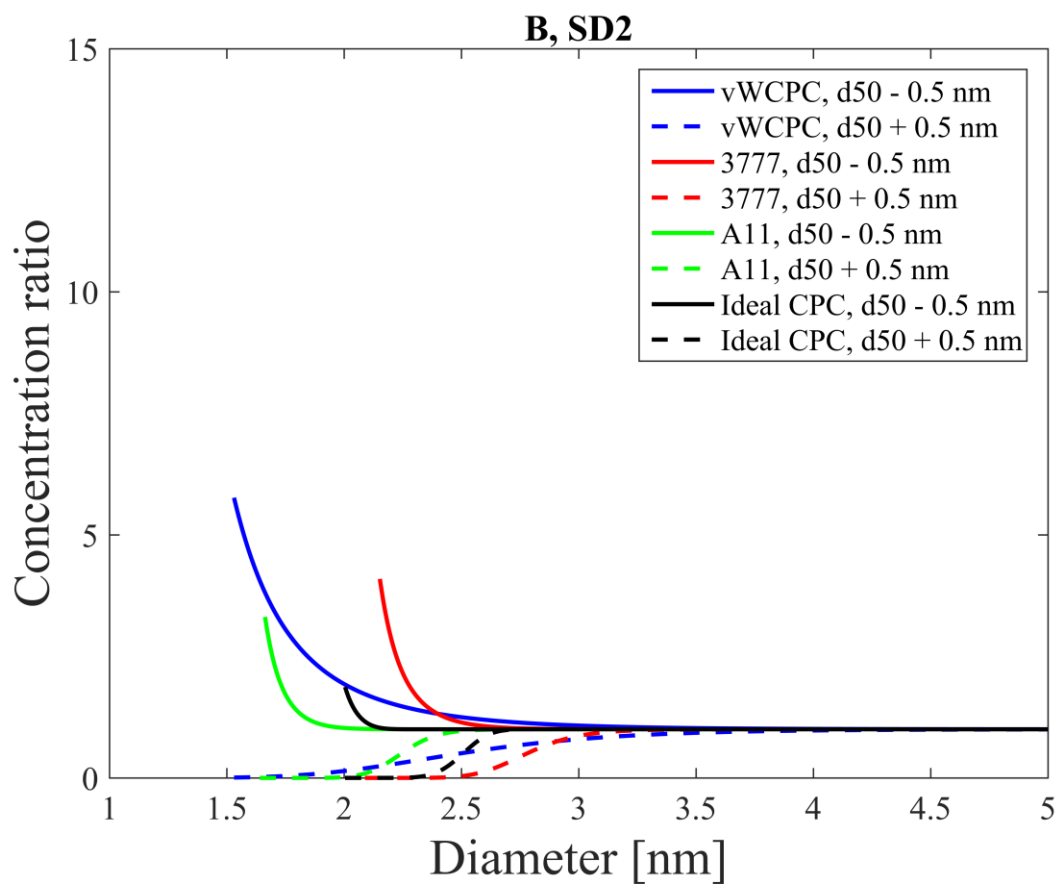
685



686
 687 Figure 7. Inverted concentrations and the ratios of the inverted concentration to the initial size
 688 distributions for the case study 2, in which the size distributions were sampled with the DMA-CPC
 689 method. Note the different y-axis scales in lower panels.



690



691

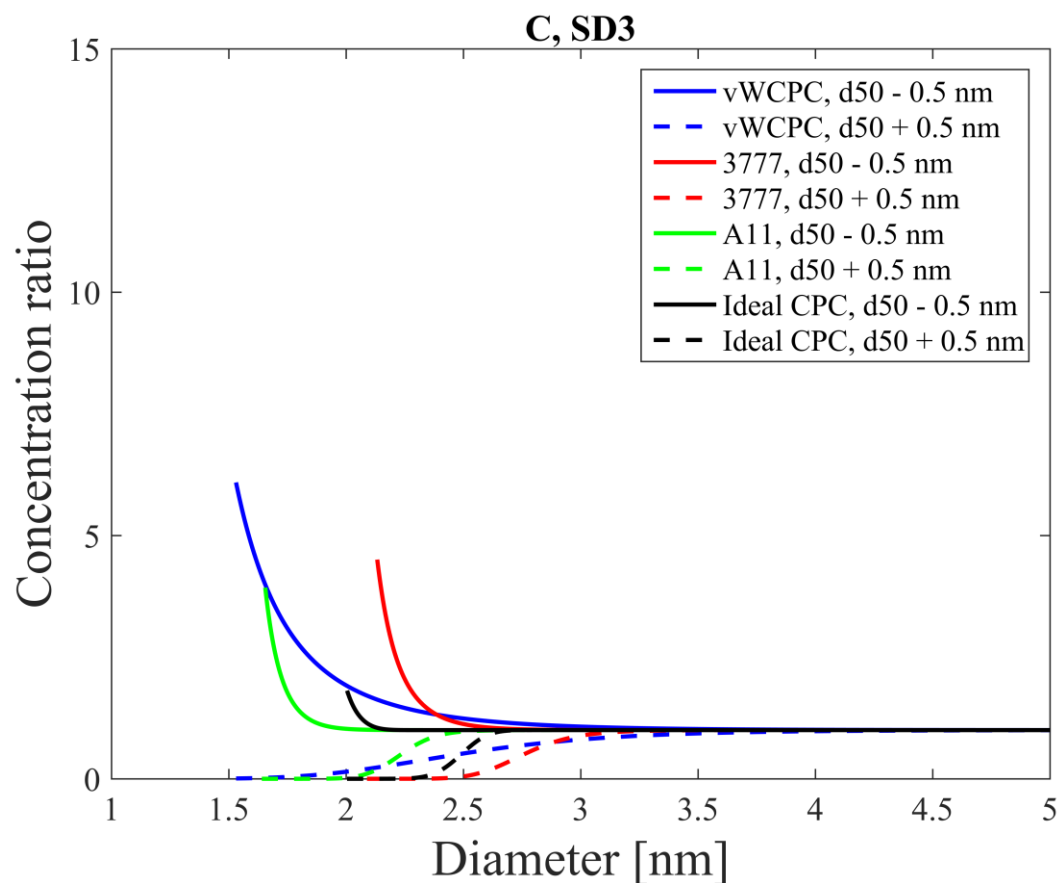
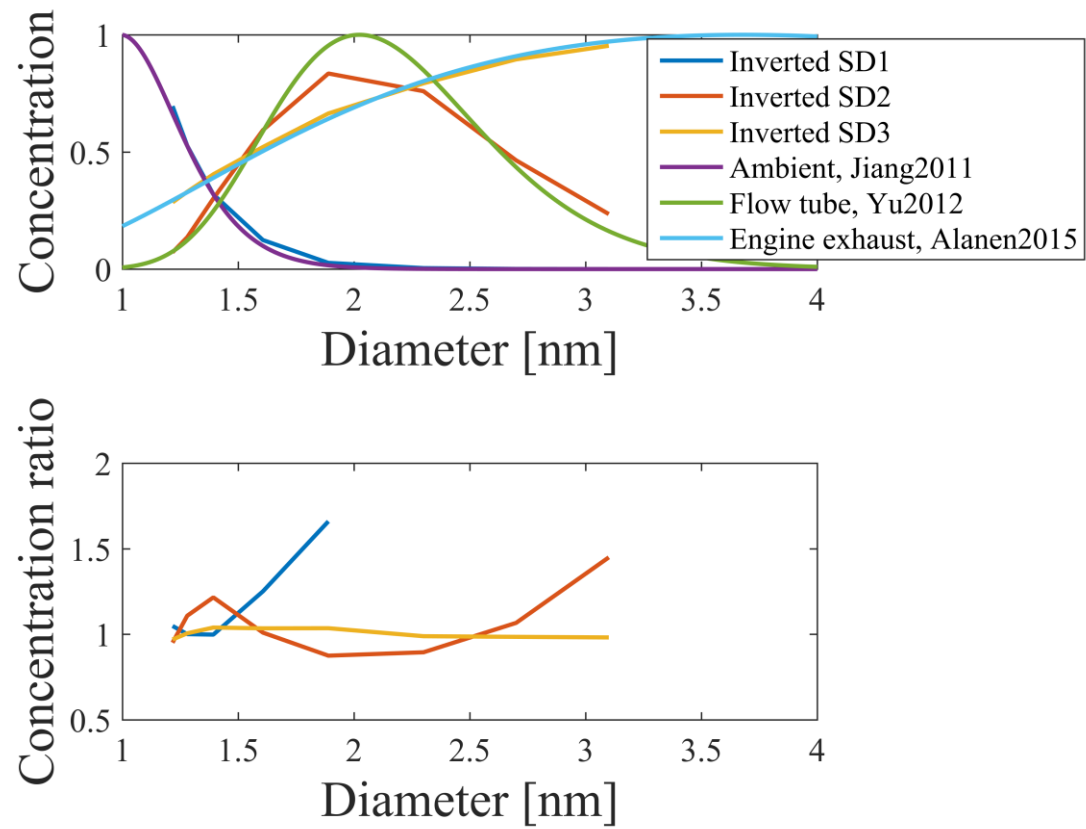
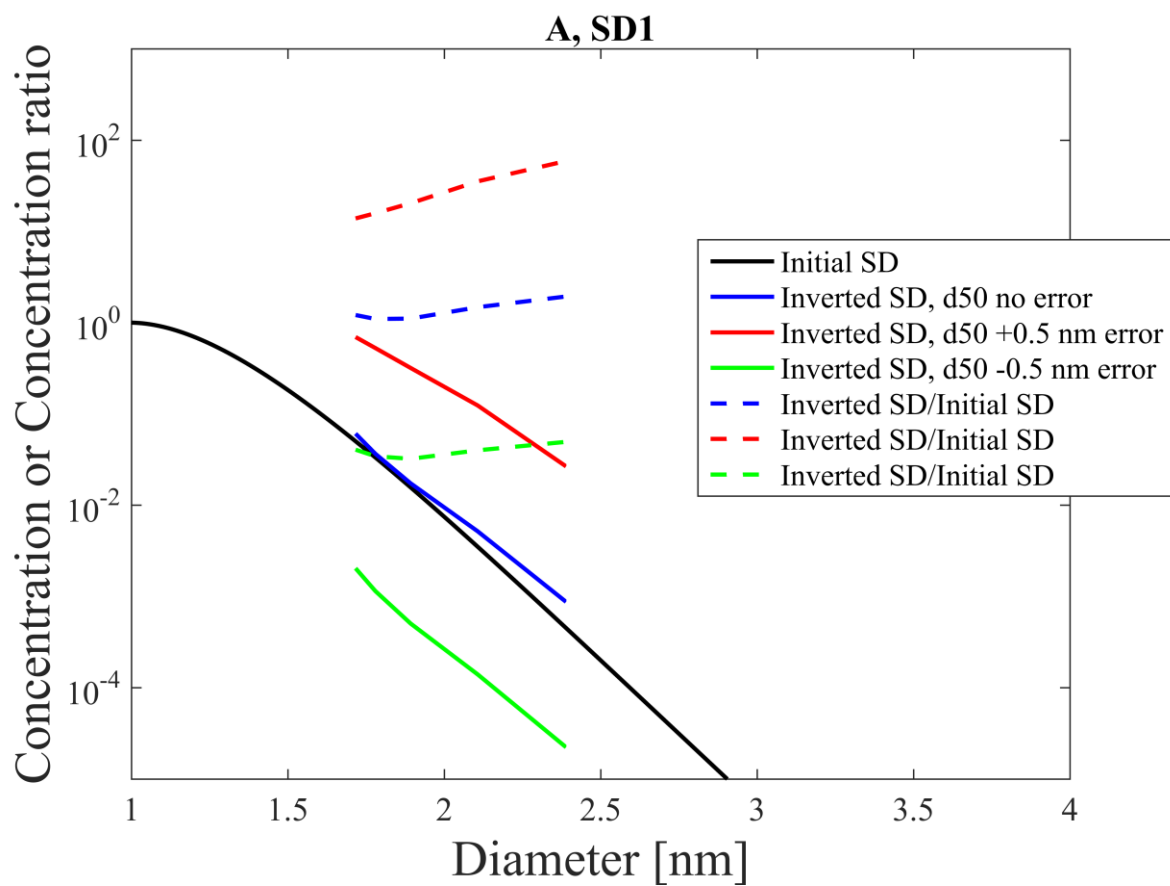


Figure 8. The ratios of inverted concentration to initial size distribution for the case study 2 in which the size distributions were sampled with the DMA-CPC method. ± 0.5 nm uncertainty is inserted to the d50 curve.

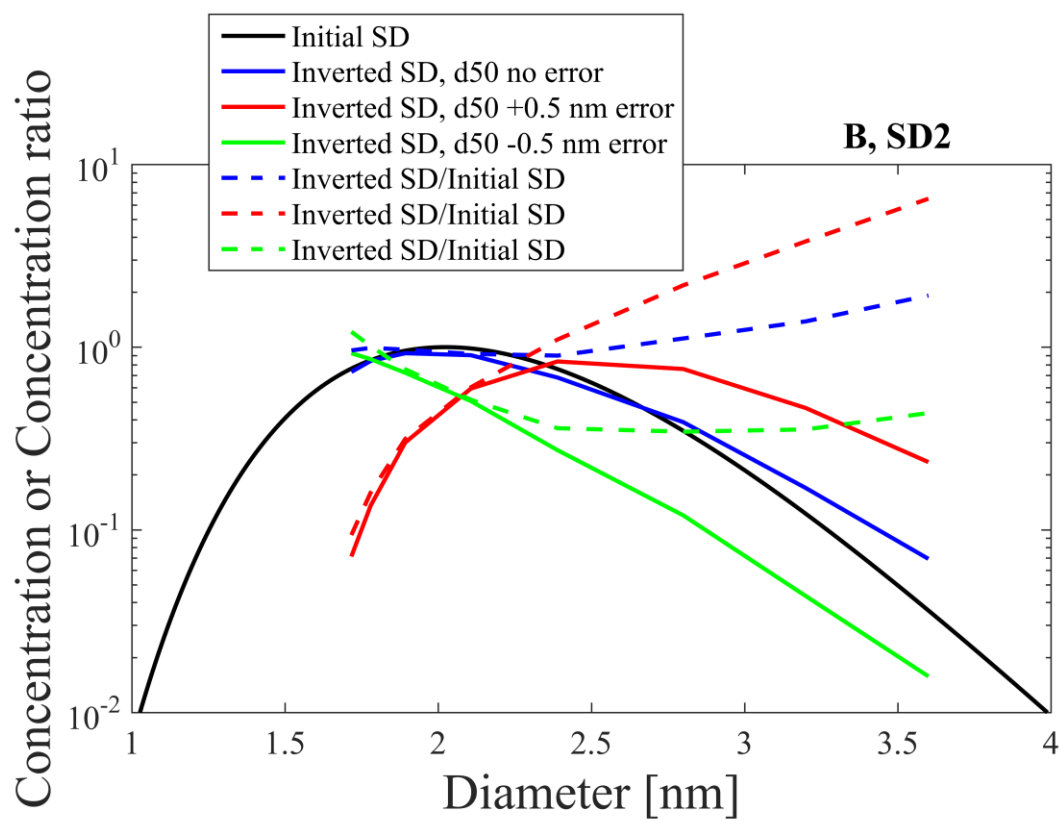


698

699 Figure 9. Inverted concentrations and the ratios of the inverted concentration to the initial size
 700 distributions in case study 4 with the PSM method.



701



702

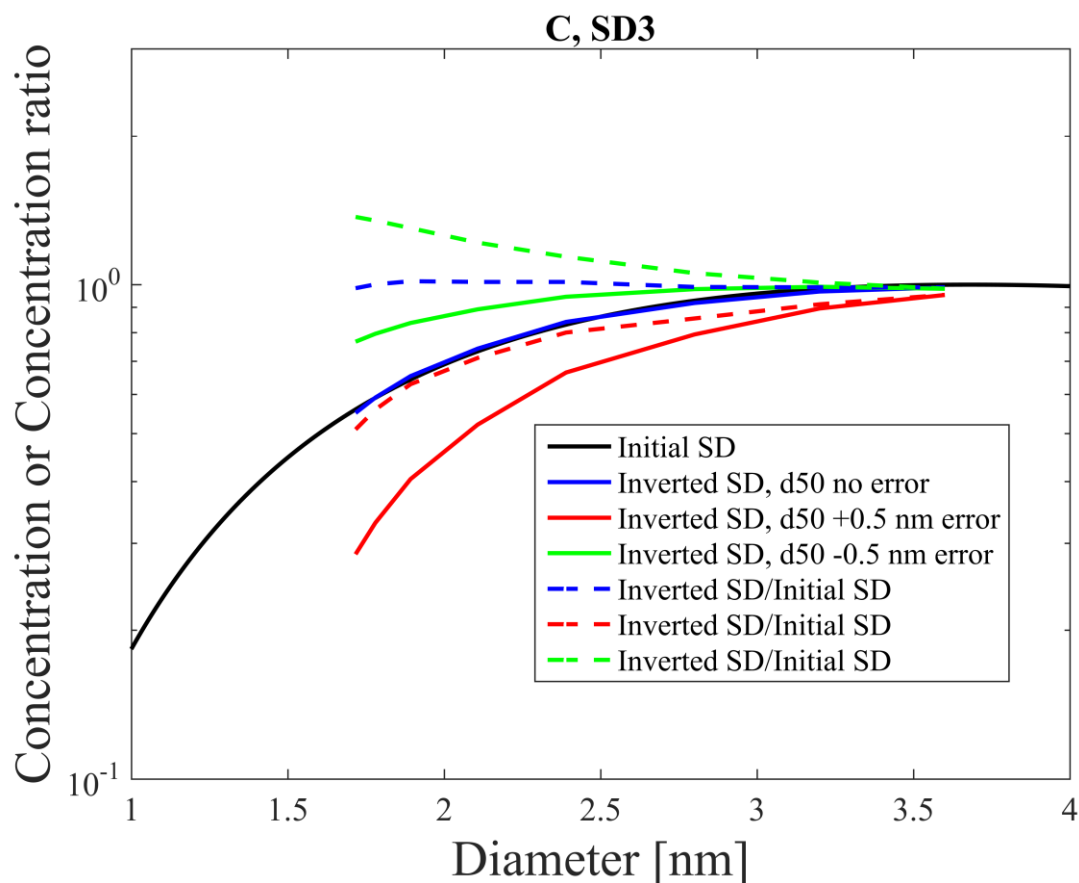


Figure 10. Inverted concentrations and the ratios for the case study 4.

Table 1. Statistical (std/mean, [%]) and Poisson (N/vN, [%]) uncertainties for the counted particles in the simulation of Figure 1.

$N_{\text{detected,vWCPC}}$	$\text{Statistical}_{\text{vWCPC}}$	$\text{Poisson}_{\text{vWCPC}}$	$N_{\text{detected,3777}}$	$\text{Statistical}_{3777}$	Poisson_{3777}	$N_{\text{detected,A11}}$	Statistical_{A11}	Poisson_{A11}
7.71	0.36	0.37	1.00	0.98	1.29	16.64	0.25	0.25
77.05	0.11	0.11	9.73	0.32	0.32	166.18	0.08	0.08
770.46	0.04	0.04	97.51	0.10	0.10	1663.40	0.02	0.02
7698.70	0.01	0.01	973.26	0.03	0.03	16629.30	0.01	0.01

Table 2. Statistical uncertainties (std/mean, [%]) for SD1 and each CPC for the parameter of Table 4 (Ratio of the detected concentration to the real concentration above the CPC d50 in Case 1)

vWCPC	3777	A11	N_{sampled}
NaN	1.41	0.18	1.00E+02
0.21	0.42	0.05	1.00E+03
0.06	0.10	0.02	1.00E+04
0.02	0.03	0.01	1.00E+05

Table 3. Statistical uncertainties (std/mean, [%]) for SD1 and each CPC for the parameter of Table 5 (Fraction of detected particles that are smaller than the nominal d50 of the CPCs for Case 1)

vWCPC	3777	A11	N_{sampled}
NaN	NaN	0.69	1.00E+02
0.16	0.64	0.21	1.00E+03

0.05 0.17 0.06 1.00E+04
0.02 0.05 0.02 1.00E+05

Table 4. Ratio of the detected concentration to the real concentration above the CPC d50 in Case 1.

Instrument	SD1	SD2	SD3
vWCPC	3.72	0.88	0.98
3777	1.32	0.96	0.99
A11	1.00	0.99	1.00
Ideal CPC	1.00	1.00	1.00

Table 5. Fraction of detected particles that are smaller than the nominal d50 of the CPCs for Case 1.

Instrument	SD1	SD2	SD3
vWCPC	0.67	0.04	0.02
3777	0.37	0.04	0.01
A11	0.12	0.00	0.00
Ideal CPC	0.00	0.00	0.00

Table 6a. Ratio of detected concentration to the real concentration above the d50 with 0.5 nm error in d50 in Case 1

Instrument	SD1	SD2	SD3
vWCPC	0.03	0.40	0.87
3777	0.02	0.27	0.87
A11	0.02	0.43	0.88
Ideal CPC	0.02	0.33	0.88

Table 6b. Ratio of detected concentration to the real concentration above the d50 with - 0.5 nm error in d50 in Case 1

Instrument	SD1	SD2	SD3
vWCPC	14.25	1.69	1.12
3777	42.00	2.32	1.13
A11	24.75	1.33	1.10
Ideal CPC	37.59	1.75	1.12

References

Alanen, J., Saukko, E., Lehtoranta, K., Murtonen, T., Timonen, H., Hillamo, R., Karjalainen, P., Kuuluvainen, H., Harra, J., Keskinen, J., and Rönkkö, T.: The formation and physical properties of the particle emissions from a natural gas engine, Fuel, 162, 155-161, 2015.

Almeida, J., Schobesberger, S., Kurten, A., Ortega, I. K., Kupiainen-Määttä, O., Praplan, A. P., Adamov, A., Amorim, A., Bianchi, F., Breitenlechner, M., David, A., Dommen, J., Donahue, N. M., Downard, A.,

Dunne, E., Duplissy, J., Ehrhart, S., Flagan, R. C., Franchin, A., Guida, R., Hakala, J., Hansel, A., Heinritzi, M., Henschel, H., Jokinen, T., Junninen, H., Kajos, M., Kangasluoma, J., Keskinen, H., Kupc, A., Kurten, T., Kvashin, A. N., Laaksonen, A., Lehtipalo, K., Leiminger, M., Leppä, J., Loukonen, V., Makhmutov, V., Mathot, S., McGrath, M. J., Nieminen, T., Olenius, T., Onnela, A., Petäjä, T., Riccobono, F., Riipinen, I., Rissanen, M., Rondo, L., Ruuskanen, T., Santos, F. D., Sarnela, N., Schallhart, S., Schnitzhofer, R., Seinfeld, J. H., Simon, M., Sipilä, M., Stozhkov, Y., Stratmann, F., Tome, A., Tröstl, J., Tsagkogeorgas, G., Vaattovaara, P., Viisanen, Y., Virtanen, A., Vrtala, A., Wagner, P. E., Weingartner, E., Wex, H., Williamson, C., Wimmer, D., Ye, P. L., Yli-Juuti, T., Carslaw, K. S., Kulmala, M., Curtius, J., Baltensperger, U., Worsnop, D. R., Vehkamäki, H., and Kirkby, J.: Molecular understanding of sulphuric acid-amine particle nucleation in the atmosphere, *Nature*, 502, 359-363, 2013.

Alonso, M., Kousaka, Y., Nomura, T., Hashimoto, N., and Hashimoto, T.: Bipolar charging and neutralization of nanometer-sized aerosol particles, *J Aerosol Sci*, 28, 1479-1490, 1997.

Bertsekas, D. and Tsitsiklis, J.: Introduction to probability, Athena Scientific, 2002. 309-319, 2002.

Bianchi, F., Tröstl, J., Junninen, H., Frege, C., Henne, S., Hoyle, C. R., Molteni, U., Herrmann, E., Adamov, A., Bukowiecki, N., Chen, X., Duplissy, J., Gysel, M., Hutterli, M., Kangasluoma, J., Kontkanen, J., Kurten, A., Manninen, H. E., Munch, S., Perakylä, O., Petäjä, T., Rondo, L., Williamson, C., Weingartner, E., Curtius, J., Worsnop, D. R., Kulmala, M., Dommen, J., and Baltensperger, U.: New particle formation in the free troposphere: A question of chemistry and timing, *Science*, 352, 1109-1112, 2016.

Carbone, F., Attoui, M., and Gomez, A.: Challenges of measuring nascent soot in flames as evidenced by high-resolution differential mobility analysis, *Aerosol Sci Tech*, 50, 740-757, 2016.

Chen, D. R., Pui, D. Y. H., Hummes, D., Fissan, H., Quant, F. R., and Sem, G. J.: Design and evaluation of a nanometer aerosol differential mobility analyzer (Nano-DMA), *J Aerosol Sci*, 29, 497-509, 1998.

Ehn, M., Thornton, J. A., Kleist, E., Sipilä, M., Junninen, H., Pullinen, I., Springer, M., Rubach, F., Tillmann, R., Lee, B., Lopez-Hilfiker, F., Andres, S., Acir, I. H., Rissanen, M., Jokinen, T., Schobesberger, S., Kangasluoma, J., Kontkanen, J., Nieminen, T., Kurten, T., Nielsen, L. B., Jorgensen, S., Kjaergaard, H. G., Canagaratna, M., Maso, M. D., Berndt, T., Petäjä, T., Wahner, A., Kerminen, V. M., Kulmala, M., Worsnop, D. R., Wildt, J., and Mentel, T. F.: A large source of low-volatility secondary organic aerosol, *Nature*, 506, 476-479, 2014.

Eisele, F. L. and Tanner, D. J.: Measurement of the Gas-Phase Concentration of H₂SO₄ and Methane Sulfonic-Acid and Estimates of H₂SO₄ Production and Loss in the Atmosphere, *J Geophys Res-Atmos*, 98, 9001-9010, 1993.

Ezell, M. J., Chen, H., Arquero, K. D., and Finlayson-Pitts, B. J.: Aerosol fast flow reactor for laboratory studies of new particle formation, *J Aerosol Sci*, 78, 30-40, 2014.

Flagan, R. C.: On differential mobility analyzer resolution, *Aerosol Sci Tech*, 30, 556-570, 1999.

776 Fletcher, N. H.: Size Effect in Heterogeneous Nucleation, J Chem Phys, 29, 572-576, 1958.

777

778 Gamero-Castano, M. and Fernández de la Mora, J.: A condensation nucleus counter (CNC) sensitive
779 to singly charged sub-nanometer particles, J Aerosol Sci, 31, 757-772, 2000.

780

781 Hering, S. V., Stolzenburg, M. R., Quant, F. R., Oberreit, D. R., and Keady, P. B.: A laminar-flow, water-
782 based condensation particle counter (WCPC), Aerosol Sci Tech, 39, 659-672, 2005.

783

784 Hering, S. V., Lewis, G. L., Spielman, S. R., Eiguren-Fernandez, A., Kreisberg, N. M., Kuang, C., and
785 Attoui, M.: Detection near 1-nm with a Laminar-Flow, Water-Based Condensation Particle Counter,
786 Aerosol Sci Tech, 2016. 2016.

787

788 Hewitt, G. W.: The charging of small particles for electrostatic precipitation, American Institute of
789 Electrical Engineers Transactions, 76, 300-306, 1957.

790

791 Iida, K., Stolzenburg, M. R., and McMurry, P. H.: Effect of Working Fluid on Sub-2 nm Particle
792 Detection with a Laminar Flow Ultrafine Condensation Particle Counter, Aerosol Sci Tech, 43, 81-96,
793 2009.

794

795 Jiang, J. K., Attoui, M., Heim, M., Brunelli, N. A., McMurry, P. H., Kasper, G., Flagan, R. C., Giapis, K.,
796 and Mouret, G.: Transfer Functions and Penetrations of Five Differential Mobility Analyzers for Sub-2
797 nm Particle Classification, Aerosol Sci Tech, 45, 480-492, 2011a.

798

799 Jiang, J. K., Chen, M. D., Kuang, C. A., Attoui, M., and McMurry, P. H.: Electrical Mobility
800 Spectrometer Using a Diethylene Glycol Condensation Particle Counter for Measurement of Aerosol
801 Size Distributions Down to 1 nm, Aerosol Sci Tech, 45, 510-521, 2011b.

802

803 Jiang, J. K., Zhao, J., Chen, M. D., Eisele, F. L., Scheckman, J., Williams, B. J., Kuang, C. A., and
804 McMurry, P. H.: First Measurements of Neutral Atmospheric Cluster and 1-2 nm Particle Number
805 Size Distributions During Nucleation Events, Aerosol Sci Tech, 45, 11-19, 2011c.

806

807 Jokinen, T., Sipilä, M., Junninen, H., Ehn, M., Lönn, G., Hakala, J., Petäjä, T., Mauldin, R. L., Kulmala,
808 M., and Worsnop, D. R.: Atmospheric sulphuric acid and neutral cluster measurements using CI-API-
809 TOF, Atmos Chem Phys, 12, 4117-4125, 2012.

810

811 Kangasluoma, J., Kuang, C., Wimmer, D., Rissanen, M. P., Lehtipalo, K., Ehn, M., Worsnop, D. R.,
812 Wang, J., Kulmala, M., and Petäjä, T.: Sub-3 nm particle size and composition dependent response of
813 a nano-CPC battery, Atmos Meas Tech, 7, 689-700, 2014.

814

815 Kangasluoma, J., Attoui, M., Junninen, H., Lehtipalo, K., Samodurov, A., Korhonen, F., Sarnela, N.,
816 Schmidt-Ott, A., Worsnop, D., Kulmala, M., and Petäjä, T.: Sizing of neutral sub 3 nm tungsten oxide
817 clusters using Airmodus Particle Size Magnifier, J Aerosol Sci, 87, 53-62, 2015.

818

819 Kangasluoma, J., Franchin, A., Duplissy, J., Ahonen, L., Korhonen, F., Attoui, M., Mikkilä, J., Lehtipalo,
820 K., Vanhanen, J., Kulmala, M., and Petäjä, T.: Operation of the Airmodus A11 nano Condensation
821 Nucleus Counter at various inlet pressures, various operation temperatures and design of a new inlet
822 system, *Atmos Meas Tech*, 9, 2977-2988, 2016a.

823

824 Kangasluoma, J., Samodurov, A., Attoui, M., Franchin, A., Junninen, H., Korhonen, F., Kurtén, T.,
825 Vehkamäki, H., Sipilä, M., Lehtipalo, K., Worsnop, D., Petäjä, T., and Kulmala, M.: Heterogeneous
826 nucleation onto ions and neutralized ions - insights into sign-preference, *Journal of Physical*
827 *Chemistry C*, 120, 7444-7450, 2016b.

828

829 Kangasluoma, J., Hering, S., Picard, D., Lewis, G., Enroth, J., Korhonen, F., Kulmala, M., Sellegri, K.,
830 Attoui, M., and Petäjä, T.: Characterization of three new condensation particle counters for sub 3 nm
831 particle detection: ADI versatile water CPC, TSI 3777 nano enhancer and boosted 3010, *Atmos Meas*
832 *Tech*, Accepted, 2017.

833

834 Kirkby, J., Curtius, J., Almeida, J., Dunne, E., Duplissy, J., Ehrhart, S., Franchin, A., Gagne, S., Ickes, L.,
835 Kurten, A., Kupc, A., Metzger, A., Riccobono, F., Rondo, L., Schobesberger, S., Tsagkogeorgas, G.,
836 Wimmer, D., Amorim, A., Bianchi, F., Breitenlechner, M., David, A., Dommen, J., Downard, A., Ehn,
837 M., Flagan, R. C., Haider, S., Hansel, A., Hauser, D., Jud, W., Junninen, H., Kreissl, F., Kvashin, A.,
838 Laaksonen, A., Lehtipalo, K., Lima, J., Lovejoy, E. R., Makhmutov, V., Mathot, S., Mikkilä, J.,
839 Minginette, P., Mogo, S., Nieminen, T., Onnela, A., Pereira, P., Petäjä, T., Schnitzhofer, R., Seinfeld, J.
840 H., Sipilä, M., Stozhkov, Y., Stratmann, F., Tome, A., Vanhanen, J., Viisanen, Y., Vrtala, A., Wagner, P.
841 E., Walther, H., Weingartner, E., Wex, H., Winkler, P. M., Carslaw, K. S., Worsnop, D. R.,
842 Baltensperger, U., and Kulmala, M.: Role of sulphuric acid, ammonia and galactic cosmic rays in
843 atmospheric aerosol nucleation, *Nature*, 476, 429-433, 2011.

844

845 Kirkby, J., Duplissy, J., Sengupta, K., Frege, C., Gordon, H., Williamson, C., Heinritzi, M., Simon, M.,
846 Yan, C., Almeida, J., Tröstl, J., Nieminen, T., Ortega, I. K., Wagner, R., Adamov, A., Amorim, A.,
847 Bernhammer, A. K., Bianchi, F., Breitenlechner, M., Brilke, S., Chen, X. M., Craven, J., Dias, A.,
848 Ehrhart, S., Flagan, R. C., Franchin, A., Fuchs, C., Guida, R., Hakala, J., Hoyle, C. R., Jokinen, T.,
849 Junninen, H., Kangasluoma, J., Kim, J., Krapf, M., Kurten, A., Laaksonen, A., Lehtipalo, K.,
850 Makhmutov, V., Mathot, S., Molteni, U., Onnela, A., Perakylä, O., Piel, F., Petäjä, T., Praplan, A. P.,
851 Pringle, K., Rap, A., Richards, N. A. D., Riipinen, I., Rissanen, M. P., Rondo, L., Sarnela, N.,
852 Schobesberger, S., Scott, C. E., Seinfeld, J. H., Sipilä, M., Steiner, G., Stozhkov, Y., Stratmann, F.,
853 Tome, A., Virtanen, A., Vogel, A. L., Wagner, A. C., Wagner, P. E., Weingartner, E., Wimmer, D.,
854 Winkler, P. M., Ye, P. L., Zhang, X., Hansel, A., Dommen, J., Donahue, N. M., Worsnop, D. R.,
855 Baltensperger, U., Kulmala, M., Carslaw, K. S., and Curtius, J.: Ion-induced nucleation of pure
856 biogenic particles, *Nature*, 533, 521-526, 2016.

857

858 Knutson, E. and Whitby, K.: Aerosol classification by electric mobility: apparatus, theory, and
859 applications, *J Aerosol Sci*, 6, 443-451, 1975.

860

861 Kontkanen, J., Järvinen, E., Manninen, H., Lehtipalo, K., Kangasluoma, J., Decesari, S., Gobbi, G. P.,
862 Laaksonen, A., Petäjä, T., and Kulmala, M.: High concentrations of sub-3nm clusters and frequent
863 new particle formation observed in the Po Valley, Italy, during the PEGASOS 2012 campaign, *Atmos*
864 *Chem Phys*, 16, 1919-1935, 2016.

865

866 Kontkanen, J., Lehtipalo, K., Ahonen, L., Kangasluoma, J., Manninen, H. E., Hakala, J., Rose, C.,
867 Sellegri, K., Xiao, S., Wang, L., Qi, X., Nie, W., Ding, A., Yu, H., Lee, S., Kerminen, V. M., Petäjä, T., and
868 Kulmala, M.: Measurements of sub-3 nm particles using Particle Size Magnifier in different
869 environments: from clean mountain top to polluted megacities, *Atmos Chem Phys*, 17, 2163-2187,
870 2017.

871

872 Kuang, C., Chen, M., Zhao, J., Smith, J., McMurry, P. H., and Wang, J.: Size and time-resolved growth
873 rate measurements of 1 to 5 nm freshly formed atmospheric nuclei, *Atmos Chem Phys*, 12, 3573-
874 3589, 2012.

875

876 Kulmala, M., Petäjä, T., Nieminen, T., Sipilä, M., Manninen, H. E., Lehtipalo, K., Dal Maso, M., Aalto,
877 P. P., Junninen, H., Paasonen, P., Riipinen, I., Lehtinen, K. E. J., Laaksonen, A., and Kerminen, V. M.:
878 Measurement of the nucleation of atmospheric aerosol particles, *Nat Protoc*, 7, 1651-1667, 2012.

879

880 Kulmala, M., Kontkanen, J., Junninen, H., Lehtipalo, K., Manninen, H. E., Nieminen, T., Petäjä, T.,
881 Sipilä, M., Schobesberger, S., Rantala, P., Franchin, A., Jokinen, T., Järvinen, E., Äijälä, M.,
882 Kangasluoma, J., Hakala, J., Aalto, P. P., Paasonen, P., Mikkilä, J., Vanhanen, J., Aalto, J., Hakola, H.,
883 Makkonen, U., Ruuskanen, T., Mauldin, R. L., Duplissy, J., Vehkamäki, H., Bäck, J., Kortelainen, A.,
884 Riipinen, I., Kurten, T., Johnston, M. V., Smith, J. N., Ehn, M., Mentel, T. F., Lehtinen, K. E. J.,
885 Laaksonen, A., Kerminen, V. M., and Worsnop, D. R.: Direct Observations of Atmospheric Aerosol
886 Nucleation, *Science*, 339, 943-946, 2013.

887

888 Kulmala, M., Petäjä, T., Ehn, M., Thornton, J., Sipilä, M., Worsnop, D. R., and Kerminen, V. M.:
889 Chemistry of Atmospheric Nucleation: On the Recent Advances on Precursor Characterization and
890 Atmospheric Cluster Composition in Connection with Atmospheric New Particle Formation, *Annu*
891 *Rev Phys Chem*, 65, 21-37, 2014.

892

893 Lehtipalo, K., Leppä, J., Kontkanen, J., Kangasluoma, J., Franchin, A., Wimmer, D., Schobesberger, S.,
894 Junninen, H., Petäjä, T., Sipilä, M., Mikkilä, J., Vanhanen, J., Worsnop, D. R., and Kulmala, M.:
895 Methods for determining particle size distribution and growth rates between 1 and 3 nm using the
896 Particle Size Magnifier, *Boreal Environ Res*, 19, 215-236, 2014.

897

898 Lehtipalo, K., Rondo, L., Kontkanen, J., Schobesberger, S., Jokinen, T., Sarnela, N., Kurten, A., Ehrhart,
899 S., Franchin, A., Nieminen, T., Riccobono, F., Sipilä, M., Yli-Juuti, T., Duplissy, J., Adamov, A., Ahlm, L.,
900 Almeida, J., Amorim, A., Bianchi, F., Breitenlechner, M., Dommen, J., Downard, A. J., Dunne, E. M.,
901 Flagan, R. C., Guida, R., Hakala, J., Hansel, A., Jud, W., Kangasluoma, J., Kerminen, V. M., Keskinen,
902 H., Kim, J., Kirkby, J., Kupc, A., Kupiainen-Maatta, O., Laaksonen, A., Lawler, M. J., Leiminger, M.,
903 Mathot, S., Olenius, T., Ortega, I. K., Onnela, A., Petaja, T., Praplan, A., Rissanen, M. P., Ruuskanen,
904 T., Santos, F. D., Schallhart, S., Schnitzhofer, R., Simon, M., Smith, J. N., Trostl, J., Tsagkogeorgas, G.,
905 Tome, A., Vaattovaara, P., Vehkamäki, H., Vrtala, A. E., Wagner, P. E., Williamson, C., Wimmer, D.,
906 Winkler, P. M., Virtanen, A., Donahue, N. M., Carslaw, K. S., Baltensperger, U., Riipinen, I., Curtius, J.,
907 Worsnop, D. R., and Kulmala, M.: The effect of acid-base clustering and ions on the growth of
908 atmospheric nano-particles, *Nat Commun*, 7, 2016.

909

910 Lindinger, W., Hansel, A., and Jordan, A.: Proton-transfer-reaction mass spectrometry (PTR-MS): on-
911 line monitoring of volatile organic compounds at pptv levels, *Chem Soc Rev*, 27, 347-354, 1998.

912

913 Lopez-Hilfiker, F. D., Mohr, C., Ehn, M., Rubach, F., Kleist, E., Wildt, J., Mentel, T. F., Carrasquillo, A. J.,
 914 Daumit, K. E., Hunter, J. F., Kroll, J. H., Worsnop, D. R., and Thornton, J. A.: Phase partitioning and
 915 volatility of secondary organic aerosol components formed from alpha-pinene ozonolysis and OH
 916 oxidation: the importance of accretion products and other low volatility compounds, *Atmos Chem*
 917 *Phys*, 15, 7765-7776, 2015.

918
 919 Nosko, O., Vanhanen, J., and Olofsson, U.: Emission of 1.3–10 nm airborne particles from brake
 920 materials, *Aerosol Sci Tech*, 51, 91-96, 2016.

921
 922 Okuyama, K., Kousaka, Y., and Motouchi, T.: Condensational Growth of Ultrafine Aerosol-Particles in
 923 a New Particle-Size Magnifier, *Aerosol Sci Tech*, 3, 353-366, 1984.

924
 925 Premnath, V., Oberreit, D., and Hogan, C. J.: Collision-Based Ionization: Bridging the Gap between
 926 Chemical Ionization and Aerosol Particle Diffusion Charging, *Aerosol Sci Tech*, 45, 712-726, 2011.

927
 928 Seto, T., Okuyama, K., de Juan, L., and Fernández de la Mora, J.: Condensation of supersaturated
 929 vapors on monovalent and divalent ions on varying size, *J Chem Phys*, 107, 1576-1585, 1997.

930
 931 Sipilä, M., Sarnela, N., Jokinen, T., Henschel, H., Junninen, H., Kontkanen, J., Richters, S.,
 932 Kangasluoma, J., Franchin, A., Perakylä, O., Rissanen, M. P., Ehn, M., Vehkamäki, H., Kurten, T.,
 933 Berndt, T., Petäjä, T., Worsnop, D., Ceburnis, D., Kerminen, V. M., Kulmala, M., and O'Dowd, C.:
 934 Molecular-scale evidence of aerosol particle formation via sequential addition of HIO₃, *Nature*, 537,
 935 532-534, 2016.

936
 937 Smith, J. N., Barsanti, K. C., Friedli, H. R., Ehn, M., Kulmala, M., Collins, D. R., Scheckman, J. H.,
 938 Williams, B. J., and McMurry, P. H.: Observations of aminium salts in atmospheric nanoparticles and
 939 possible climatic implications, *P Natl Acad Sci USA*, 107, 6634-6639, 2010.

940
 941 Stolzenburg, M. R. and McMurry, P. H.: An Ultrafine Aerosol Condensation Nucleus Counter, *Aerosol*
 942 *Sci Tech*, 14, 48-65, 1991.

943
 944 Stolzenburg, M. R. and McMurry, P. H.: Equations governing single and tandem DMA configurations
 945 and a new lognormal approximation to the transfer function, *Aerosol Sci Tech*, 42, 421-432, 2008.

946
 947 Tröstl, J., Chuang, W. K., Gordon, H., Heinritzi, M., Yan, C., Molteni, U., Ahlm, L., Frege, C., Bianchi, F.,
 948 Wagner, R., Simon, M., Lehtipalo, K., Williamson, C., Craven, J. S., Duplissy, J., Adamov, A., Almeida,
 949 J., Bernhammer, A. K., Breitenlechner, M., Brilke, S., Dias, A., Ehrhart, S., Flagan, R. C., Franchin, A.,
 950 Fuchs, C., Guida, R., Gysel, M., Hansel, A., Hoyle, C. R., Jokinen, T., Junninen, H., Kangasluoma, J.,
 951 Keskinen, H., Kim, J., Krapf, M., Kurten, A., Laaksonen, A., Lawler, M., Leiminger, M., Mathot, S.,
 952 Mohler, O., Nieminen, T., Onnela, A., Petäjä, T., Piel, F. M., Miettinen, P., Rissanen, M. P., Rondo, L.,
 953 Sarnela, N., Schobesberger, S., Sengupta, K., Sipilä, M., Smith, J. N., Steiner, G., Tome, A., Virtanen,
 954 A., Wagner, A. C., Weingartner, E., Wimmer, D., Winkler, P. M., Ye, P. L., Carslaw, K. S., Curtius, J.,
 955 Dommen, J., Kirkby, J., Kulmala, M., Riipinen, I., Worsnop, D. R., Donahue, N. M., and Baltensperger,
 956 U.: The role of low-volatility organic compounds in initial particle growth in the atmosphere, *Nature*,
 957 533, 527-531, 2016.

958

959 Vanhanen, J., Mikkilä, J., Lehtipalo, K., Sipilä, M., Manninen, H. E., Siivola, E., Petäjä, T., and Kulmala,
960 M.: Particle Size Magnifier for Nano-CN Detection, *Aerosol Sci Tech*, 45, 533-542, 2011.

961

962 Wang, Y., Kangasluoma, J., Attoui, M., Fang, J., Junninen, H., Kulmala, M., Petäjä, T., and Biswas, P.:
963 Observation of incipient particle formation during flame synthesis by tandem differential mobility
964 analysis-mass spectrometry (DMA-MS), *Proceedings of the Combustion Institute* (in press), 2016. 1-
965 8, 2016.

966

967 Wang, Y., Kangasluoma, J., Attoui, M., Fang, J., Junninen, H., Kulmala, M., Petäjä, T., and Biswas, P.:
968 The high charge fraction of flame-generated particles in the size range below 3 nm measured by
969 enhanced particle detectors, *Combust Flame*, 176, 72-80, 2017.

970

971 Wiedensohler, A. and Fissan, H. J.: Bipolar Ion and Electron-Diffusion Charging of Aerosol-Particles in
972 High-Purity Argon and Nitrogen, *Particle & Particle Systems Characterization*, 7, 250-255, 1990.

973

974 Wiedensohler, A., Birmili, W., Nowak, A., Sonntag, A., Weinhold, K., Merkel, M., Wehner, B., Tuch, T.,
975 Pfeifer, S., Fiebig, M., Fjaraa, A. M., Asmi, E., Sellegri, K., Depuy, R., Venzac, H., Villani, P., Laj, P.,
976 Aalto, P., Ogren, J. A., Swietlicki, E., Williams, P., Roldin, P., Quincey, P., Huglin, C., Fierz-
977 Schmidhauser, R., Gysel, M., Weingartner, E., Riccobono, F., Santos, S., Gruning, C., Faloon, K.,
978 Beddows, D., Harrison, R. M., Monahan, C., Jennings, S. G., O'Dowd, C. D., Marinoni, A., Horn, H. G.,
979 Keck, L., Jiang, J., Scheckman, J., McMurry, P. H., Deng, Z., Zhao, C. S., Moerman, M., Henzing, B., de
980 Leeuw, G., Loschau, G., and Bastian, S.: Mobility particle size spectrometers: harmonization of
981 technical standards and data structure to facilitate high quality long-term observations of
982 atmospheric particle number size distributions, *Atmos Meas Tech*, 5, 657-685, 2012.

983

984 Wimmer, D., Lehtipalo, K., Franchin, A., Kangasluoma, J., Kreissl, F., Kurten, A., Kupc, A., Metzger, A.,
985 Mikkilä, J., Petäjä, T., Riccobono, F., Vanhanen, J., Kulmala, M., and Curtius, J.: Performance of
986 diethylene glycol-based particle counters in the sub-3 nm size range, *Atmos Meas Tech*, 6, 1793-
987 1804, 2013.

988

989 Winkler, P. M., Steiner, G., Vrtala, A., Vehkamäki, H., Noppel, M., Lehtinen, K. E. J., Reischl, G. P.,
990 Wagner, P. E., and Kulmala, M.: Heterogeneous nucleation experiments bridging the scale from
991 molecular ion clusters to nanoparticles, *Science*, 319, 1374-1377, 2008.

992

993 Yu, H., McGraw, R., and Lee, S. H.: Effects of amines on formation of sub-3 nm particles and their
994 subsequent growth, *Geophys Res Lett*, 39, 2012.

995

996 Yu, H., Gannet Hallar, A., You, Y., Sedlacek, A., Springston, S., Kanawade, V., Lee, Y. N., Wang, J.,
997 Kuang, C., McGraw, R. L., McCubbin, I., Mikkilä, J., and Lee, S. H.: Sub-3 nm particles observed at the
998 coastal and continental sites in the United States, *Journal of Geophysical Research: Atmospheres*,
999 119, 860-879, 2014.

1000

1001